

NAVAL POSTGRADUATE SCHOOL

Monterey, California



THESIS

**SIMULATION OF DARMSTADT FREE ELECTRON
LASER AND A COMPARISON OF HIGH GAIN FREE
ELECTRON LASERS**

by

Daniel S. Massey

December 2000

Thesis Advisor:
Second Reader:

William B. Colson
Robert L. Armstead

Approved for public release; distribution is unlimited.

20010316 067

REPORT DOCUMENTATION PAGE

Form Approved
OMB No. 0704-0188

Public reporting burden for this collection of information is estimated to average 1 hour per response, including the time for reviewing instruction, searching existing data sources, gathering and maintaining the data needed, and completing and reviewing the collection of information. Send comments regarding this burden estimate or any other aspect of this collection of information, including suggestions for reducing this burden, to Washington headquarters Services, Directorate for Information Operations and Reports, 1215 Jefferson Davis Highway, Suite 1204, Arlington, VA 22202-4302, and to the Office of Management and Budget, Paperwork Reduction Project (0704-0188) Washington DC 20503.

1. AGENCY USE ONLY (Leave blank)

2. REPORT DATE
December 2000

3. REPORT TYPE AND DATES COVERED
Master's Thesis

4. TITLE AND SUBTITLE

Simulation Of Darmstadt Free Electron Laser and a Comparison of High Gain Free Electron Lasers

5. FUNDING NUMBERS

6. AUTHOR(S)

Massey, Daniel S.

7. PERFORMING ORGANIZATION NAME(S) AND ADDRESS(ES)

Naval Postgraduate School
Monterey, CA 93943-5000

8. PERFORMING
ORGANIZATION REPORT
NUMBER

9. SPONSORING / MONITORING AGENCY NAME(S) AND ADDRESS(ES)

10. SPONSORING /
MONITORING
AGENCY REPORT NUMBER

11. SUPPLEMENTARY NOTES

The views expressed in this thesis are those of the author and do not reflect the official policy or position of the Department of Defense or the U.S. Government.

12a. DISTRIBUTION / AVAILABILITY STATEMENT

Approved for public release; distribution is unlimited.

12b. DISTRIBUTION CODE

13. ABSTRACT (maximum 200 words)

The Free Electron Laser, with its wavelength tunability unlike any other laser, may be used in numerous future applications. These applications range from high energy laser weapons to surgical lasers for medical use. This thesis covers three separate topics concerning the FEL: the height of the separatrix for a tapered undulator, use of dimensionless parameters in a simple model and description for several high gain free electron lasers, and simulations of the Darmstadt free electron laser. The first topic yielded a formula for the separatrix height. The second topic utilized data from the proposed LCLS and TESLA x-ray lasers, the Electron Laser Facility at Lawrence Livermore Labs and the Free Electron Laser experiments at the Massachusetts Institute of Technology to develop dimensionless parameters for use in a simple model. For the last topic desynchronism curves for seven tapers were computed and gave expected results.

14. SUBJECT TERMS

Free Electron Laser

15. NUMBER OF
PAGES

88

16. PRICE CODE

17. SECURITY CLASSIFICATION OF
REPORT

Unclassified

18. SECURITY CLASSIFICATION OF
THIS PAGE

Unclassified

19. SECURITY CLASSIFI- CATION
OF ABSTRACT

Unclassified

20. LIMITATION
OF ABSTRACT

UL

Approved for public release; distribution is unlimited

**SIMULATION OF DARMSTADT FREE ELECTRON LASER AND A
COMPARISON OF HIGH GAIN FREE ELECTRON LASER**

Daniel S. Massey
Lieutenant, United States Navy
B.S., United States Naval Academy, 1994

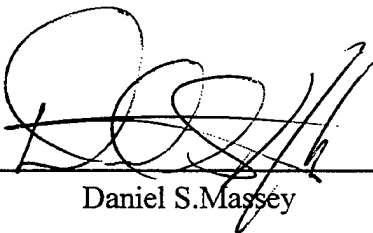
Submitted in partial fulfillment of the
requirements for the degree of

MASTER OF SCIENCE IN PHYSICS

from the

**NAVAL POSTGRADUATE SCHOOL
December 2000**

Author:



Daniel S. Massey

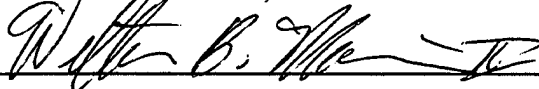
Approved by:



William B. Colson, Thesis Advisor



Robert L. Armstead, Second Reader



William Maier II, Chairman
Department of Physics

TABLE OF CONTENT

I.	INTRODUCTION.....	1
II.	BACKGROUND THEORY	3
A.	INITIAL CONDITIONS.....	3
1.	Undulator Field.....	3
2.	Initial Optical Field.....	5
B.	ELECTRON DYNAMICS	5
1.	The Electron Phase.....	5
2.	Wavelength of Light in FEL.....	6
3.	Electron Paths.....	7
C.	ELECTRON PENDULUM EQUATION.....	11
D.	OPTICAL WAVE EQUATION	15
E.	GAIN MECHANISMS.....	18
1.	Phase Space.....	19
2.	Separatrix.....	20
3.	Bunching.....	21
4.	Changes in Phase Velocity.....	22
5.	Gain Formula.....	22
6.	Low Gain.....	23
7.	High Gain.....	24
F.	BEAM QUALITY	25
G.	SHORT PULSE EFFECTS.....	27
H.	TAPER	29
1.	Purpose of Taper.....	29
2.	Taper Phase Space.....	30
III.	TAPER SEPARATRIX HEIGHT	33
A.	POSITIVE TAPER.....	34
B.	NEGATIVE TAPER.....	35
C.	POSTIVE AND NEGATIVE TAPER.....	36
D.	LINEAR APPROXIMATION.....	37
IV.	PARAMETERS FOR USE IN SIMPLE MODEL OF A HIGH GAIN FEL.....	39
A.	DESCRIPTION OF LCLS AT SLAC.....	40
B.	TESLA FEL AT DESY	41
C.	ANALYSIS OF SLAC AND TESLA PARAMETERS	41
1.	Wavelength.....	41
2.	Reducing j	42
3.	Rayleigh Length.....	43
4.	Emittance.....	45
5.	Slip.....	46
6.	Initial Optical Field.....	46
D.	ELECTRON LASER FACILITY (ELF).....	47
E.	ELF85.....	48
1.	Electron Beam to Optical Field Ratio the Filling Factor.....	48
2.	Slip.....	49
3.	Emittance.....	49
F.	ELF 86.....	49

1. <i>Electron Beam to Optical Field Ratio, the Filling Factor</i>	50
G. ELF87.....	50
H. MIT FEL	51
1. <i>Natural Focusing</i>	52
2. <i>SASE</i>	52
3. <i>Electron Beam</i>	52
I. CONCLUSION.....	53
V. DARMSTADT FEL	55
A. DARMSTADT PARAMETERS	55
B. BEAM SIZE EFFECTS ON GAIN	56
1. <i>Theoretical Background</i>	56
2. <i>Method of Analysis</i>	57
C. TAPER EFFECTS	61
1. <i>Compiled Data</i>	61
2. <i>Untapered Power Curve Analysis</i>	64
3. <i>Simulation</i>	65
4. <i>Limit-Cycle Behavior in the Untapered case</i>	67
5. <i>Limit-Cycle Behavior in the Negative Tapered Case</i>	68
D. CONCLUSION	71
LIST OF REFERENCES	73
INITIAL DISTRIBUTION LIST	75

LIST OF SYMBOLS

A	optical vector potential
a	dimensionless optical field
B	magnetic Field
c	speed of light
d	desynchronism
E	electric Field
e	charge of electron
I	current
J	current density
j	dimensionless current
K	dimensionless undulator parameter
KE	kinetic energy
k	optical wavenumber
k_0	undulator wavenumber
L	undulator length
l_e	electron pulse length
t	time
m	mass of electron
N	number of undulator periods
n	number of passes
F	Filling Factor
N_β	Number of betatron oscillations
r_e	electron beam radius
S	resonator length
v	velocity
w	optical beam width
x	axial-position
y	axial-position
z	axial-position/ after page 30 z is dimensionless
z_0	Rayleigh length
β	v/c
γ	Lorentz factor
λ	optical wavelength
λ_0	undulator wavelength
ω	optical angular frequency
ω_β	betatron frequency
ϕ	optical phase
δ	taper
τ	dimensionless time
ζ	electron phase
v	electron phase velocity
θ	initial angle
ρ	electron density

σ_x	dimensionless l_e
σ_θ	angular spread
σ_G	phase velocity spread
ε	emittance

I. INTRODUCTION

Free Electron Lasers (FEL) may have an impact on the United States Navy, not just as a weapon, but in many fields of science such as Medicine and Physics. The tunability and high power output of a FEL makes it useful for a broad range of applications.

As a weapon, the tunability allows the user to select the frequency that will propagate most efficiently through the atmosphere. Also, the FEL has the potential to produce the power level needed for use as a weapon.

The tunability allows a doctor to select not only the wavelength, but also the pulse-repetition rate of the laser during surgery. The FEL is able to take advantage of resonant modes in a molecule to allow the doctor to precisely remove millimeter layers of skin, fat, muscle, cornea, or tumor with no collateral damage to surrounding tissue. The FEL "scalpel" may revolutionize the operating room.

The FEL is also the most viable path for achieving a coherent x-ray source. There are several projects working towards a high gain FEL that can achieve 1 angstrom x-rays. The uses for coherent x-ray sources are numerous. One use, which has a direct effect on the Navy, is to probe the reactions that occur in the initial moment of a nuclear blast.

There are numerous other uses for the FEL. Almost every field of science is finding new applications for the FEL, from probing light interactions with biological functions to studying Quantum Electro-dynamics.

This thesis covers several different FELs which have a wide range of applications. The second chapter of this thesis covers the background theory that will be used in the rest of the thesis[reference (1)]. In Chapter III I calculate analytically the height of a tapered separatrix. In Chapter IV I analyze various high gain FEL's and use some dimensionless parameters to develop a simple model for each. The final chapter I simulate the Darmstadt FEL using a computer model and analyse the results. This analysis consists of simulations at various desynchronisms that determine power and gain expected in the FEL. There are instabilities that may be experimentally observed as well.

II. BACKGROUND THEORY

The physics behind the Free Electron Laser (FEL) is based upon both spontaneous and stimulated emission from an electron. The two major components of the FEL are the relativistic electron beam and a static alternating magnetic field. The relativistic beam of electrons is accelerated in the transverse direction by the magnetic field. This acceleration initially causes spontaneous radiation from the electrons. Due to relativistic effects, the emitted light is radiated into a cone along the axis of the laser. The key to an operational FEL is the interaction between the electrons and the light field. The kinetic energy of the electron beam is converted to the radiation energy of the optical field. The electron pendulum equation and optical field equation describes the coupling.

A. INITIAL CONDITIONS

A classical approach has proven to be the most fruitful and experimental results agree with the classical results.[reference 1]

1. Undulator Field

The magnetic field of the FEL is created by a chain of fixed magnets, called an undulator. There are two basic types of undulators: helical and linear. The linear undulator is a series of bar magnets with the polarization

in alternating directions, so that an alternating magnetic field is set up. Figure 1 depicts a linear undulator with the z direction is along the axis of the laser. The magnetic field for the linear undulator is given by

$$\vec{B} = [B_x, B_y, B_z] = B_0[0, \sin(k_0 z) \cosh(k_0 y), \cos(k_0 z) \sinh(k_0 y)], \quad (\text{II-1})$$

where $k_0 = 2\pi / \lambda_0$ is the undulator wavenumber.

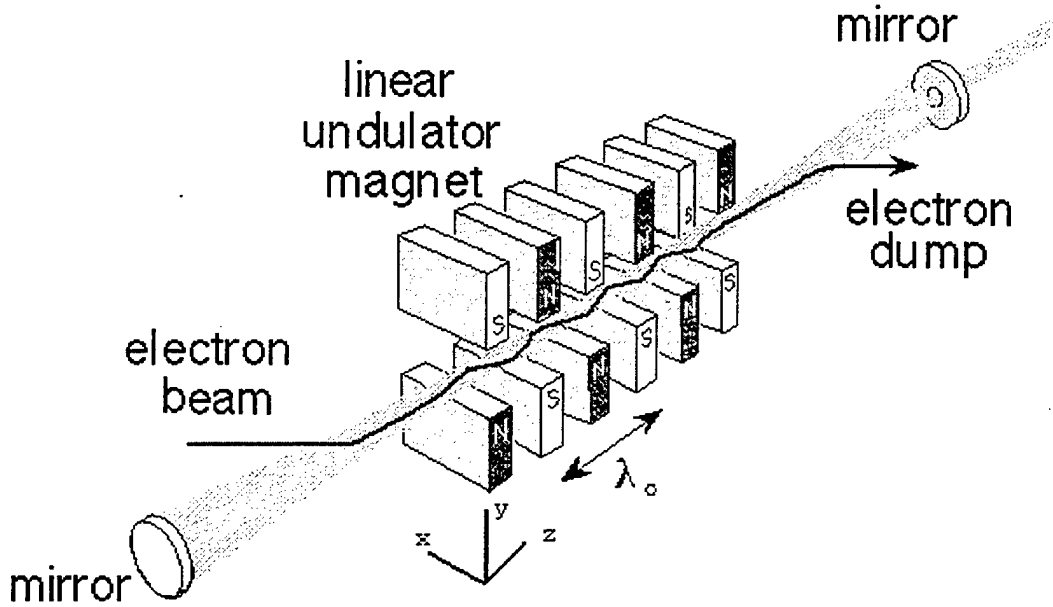


Figure II-1 Linear Undulator (after reference 7)

The helical undulator consists of two concentric currents that create a magnetic field that rotates spatially along the length of the undulator. For the helical undulator the magnetic field is given by

$$\vec{B} = B_0[\cos(k_0 z), \sin(k_0 z), 0] \quad (\text{II-2})$$

2. Initial Optical Field

To begin analyzing FEL operation we need to assume that the FEL is already operating and there is already a radiation field present. The optical field for the linear undulator is assumed to be a plainer, plane parabolic wave with the electric and magnetic fields given by $\vec{E}_s = E[\cos \psi, 0, 0]$ and $\vec{B}_s = E[0, \cos \psi, 0]$ respectively, where $\psi = kz - \omega t + \phi$. The electric field amplitude E is given in cgs units with ϕ being the optical phase and $k = 2\pi / \lambda$ is the optical wave number, $\omega = 2\pi c / \lambda$ is the optical angular frequency.

The initial optical field for the helical undulator is assumed to be a circularly polarized plane-wave. Hence the electric and magnetic fields are given by $\vec{E}_s = E[\cos \psi, -\sin \psi, 0]$ and $\vec{B}_s = E[\sin \psi, \cos \psi, 0]$, respectively.

B. ELECTRON DYNAMICS

1. The Electron Phase

Before moving on, we need to define the electron phase. The electron phase is the key to coupling the optical field with the bunching of the electron beam. In the combined undulator and light field the electron phase is defined as $\zeta(t) = (k+k_0)z(t) + \omega t$. The electron phase definition involves two fixed wave numbers $k = 2\pi / \lambda$, describing the light wave

and $k_0 = 2\pi / \lambda_0$ describing the undulator, with the only variable being $z(t)$. The electron phase follows the electron position. The time spent by the electron in the undulator is $\Delta t = L / \beta_0 c \approx L / c \approx 10^{-8} \text{ s}$, where L is the length of the undulator and the speed of the electron ($v_z = c\beta_z \approx c$) is approximately the speed of light. This time is extremely small, so it is easier to introduce a dimensionless time τ and a dimensionless time derivative

$$\tau = \frac{c\beta_z t}{L} \approx \frac{ct}{L} \quad \text{and} \quad (\dot{}) = \frac{d()}{d\tau}. \quad (\text{II-3})$$

The dimensionless time τ ranges from 0 at the beginning of the undulator to 1 at the end of the undulator ($0 \leq \tau \leq 1$). The electron phase velocity is then defined as the derivative of the electron phase

$$v(\tau) = \frac{d(\zeta)}{d\tau} = \dot{\zeta} = L[(k + k_0)\beta_z - k] \quad (\text{II-4})$$

To study the operation of the FEL, it is most informative to plot the phase velocity versus the electron phase in what is called phase-space. This will be discussed further in subsequent parts of this chapter.

2. Wavelength of Light in FEL

The traditional laser requires a bound electron to transition to a lower energy level and radiate. In the FEL, a relativistic beam of free electrons amplifies the light

wave. The undulator wavelength λ_0 is Lorentz contracted to $\lambda'_0 = \lambda_0 / \gamma$ in the electron frame. The emitted optical field is Doppler shifted is also

$$\lambda' = (1 - \beta_z)\gamma\lambda \approx 2\gamma\lambda. \quad (\text{II-5})$$

At resonance, there is optimal energy exchange. When $\lambda'_0 = \lambda'$ in the beam frame. When converted to the lab frame the resonance condition becomes

$$\lambda = \lambda_0 \frac{1 + K^2}{2\gamma^2} \quad (\text{II-6})$$

where the dimensionless undulator parameter K is defined as

$$K = \frac{e\bar{B}\lambda_0}{2\pi mc^2} = \frac{e\bar{B}}{k_0 mc^2}, \quad (\text{II-7})$$

B is the RMS magnetic field, e is the magnitude of the electron charge, m is the mass of the electron and c is the speed of light.

3. Electron Paths

To analyze the electron trajectories in the FEL, we will look at the linear undulator. The magnets are aligned along the y direction. An electron that moves off axis in the y -direction feels a stronger magnetic field because it moves closer to a magnet. The electron is pushed back toward the axis creating a natural focusing. The focusing of the undulator causes the electrons to wiggle over many undulator periods in the focused direction. The wiggle is called a

betatron oscillation. To analyze betatron effects, we will consider a perfectly injected electron in a linear undulator that focuses in the y direction. Perfect injection means that the electron is injected into a perfect sinusoidal trajectory with no angular spread.

The three spatial components are of the Lorentz force equation with the magnetic field for linear undulator from equation (II-1) as follows

$$\dot{\beta}_x = -\frac{eB}{\gamma mc} [\beta_z \sin(k_0 z) \cosh(k_0 y) - \beta_y \cos(k_0 z) \sinh(k_0 y)], \quad (\text{II-8})$$

$$\dot{\beta}_y = \frac{eB}{\gamma mc} [\beta_x \cos(k_0 z) \sinh(k_0 y)], \quad (\text{II-9})$$

$$\dot{\beta}_z = -\frac{eB}{\gamma mc} [\beta_x \sin(k_0 z) \cosh(k_0 y)]. \quad (\text{II-10})$$

In the next section, we will derive these equations in greater detail for the helical undulator. The β_x term has an exact solution, and perfect injection implies the constants of integration are set equal to zero, so

$$\beta_x = \frac{\sqrt{2}K}{\gamma} \cos(k_0 z) \cosh(k_0 y). \quad (\text{II-11})$$

Substituting β_x into the other two equations leads to

$$\dot{\beta}_y = -\frac{cK^2 k_0}{\gamma^2} \cos^2(k_0 z) \sinh(2k_0 y), \quad (\text{II-12})$$

and

$$\dot{\beta}_z = \frac{cK^2 k_0}{\gamma^2} \sin(2k_0 z) \cosh^2(k_0 y). \quad (\text{II-13})$$

Since the y and z components are coupled, we add the restriction of perfect injection in the y direction and analyze the motion in the xz -plan. Hence,

$$\beta_x = -\frac{\sqrt{2}K}{\gamma} \cos(k_0 z) \quad (\text{II-14})$$

$$\dot{\beta}_y(0) = y(0) = 0 \quad (\text{II-15})$$

$$\dot{\beta}_z = \frac{cK^2 k_0}{\gamma^2} \sin(2k_0 z) \quad (\text{II-16})$$

In the typical operating FEL $K \approx 1$ and $\gamma \gg 1$, so that $K/\gamma \ll 1$. Expand in powers of (K/γ) , so the x and z components become

$$z(t) = c\bar{\beta}_z t - \frac{K^2}{4k_0 \gamma^2} \sin(2k_0 c\bar{\beta}_z t) + \dots, \quad (\text{II-17})$$

$$x(t) = -\frac{K}{k_0 \gamma} \sin(k_0 c\bar{\beta}_z t) + \dots, \quad (\text{II-18})$$

where $\bar{\beta}_z$ is the average velocity of the electron beam in the undulator. Then converting to dimensionless time τ gives

$$z(\tau) = \bar{\beta}_z L \tau - \frac{K^2 \lambda_0}{8\pi \gamma^2} \sin(4\pi N \tau) + \dots, \quad (\text{II-19})$$

$$x(\tau) = -\frac{K \lambda_0}{\sqrt{2} \pi \gamma} \sin(2\pi N \tau) + \dots \quad (\text{II-20})$$

From these two equations, we can see that the amplitude of the transverse oscillation is $K \lambda_0 / \sqrt{2} \pi \gamma$ where the electron

oscillates once every undulator period. In the z direction, the electron oscillates twice every undulator period.

Having looked at the oscillations in the x and z directions, we now go back and assume non-perfect injection to see what happens in the y direction. The oscillations in the y direction are called betatron oscillations. Assuming small oscillations so that $k_0 y \ll 1$ and $\sinh(2k_0 y) \approx 2k_0 y$, we can rewrite equation (II-12) and convert to dimensionless parameters to get

$$\ddot{y}(\tau) = - \frac{2K^2 L^2 k_0^2}{\gamma^2} \cos^2(2\pi N \tau) y(\tau) \quad (\text{II-21})$$

Averaging over several undulator periods, since one betatron oscillation is typically over many undulator periods, we have

$$\ddot{y}(\tau) = - \frac{K^2 L^2 k_0^2}{\gamma^2} y(\tau) = -\omega_\beta^2 y(\tau). \quad (\text{II-22})$$

Equation (II-22) is the equation of motion for a simple harmonic oscillator. The solution is a well-studied sinusoidal wave, with the dimensionless betatron frequency $\omega_\beta = KLk_0/\gamma = 2\pi NK/\gamma$. The number of betatron oscillations along the undulator is

$$N_\beta = \frac{NK}{\gamma}. \quad (\text{II-23})$$

A typical value is $N_\beta \approx 1$, since $N \approx 100$, $K=1$, and $\gamma=100$ are typical values. FELs with larger values will be discussed later.

C. ELECTRON PENDULUM EQUATION

The dynamics of the FEL may be described very simply by the electron pendulum equation. The first step in deriving this equation is to consider an operating FEL where an optical field is already present. This means the electron experience forces from both the optical field and the undulator field.

The helical field is much simpler to work with mathematically and the final formulas can be converted easily to the linear case. Hence, we will just use the helical magnetic field.

The forces from the undulator field are governed by the Lorentz force equations (cgs units),

$$\frac{d\vec{p}}{dt} = \frac{d(\gamma mc \vec{\beta})}{dt} = -e(\vec{E} + \vec{\beta} \times \vec{B}), \quad (\text{II-24})$$

and the energy equation

$$\frac{d(\gamma mc^2)}{dt} = -e c \vec{\beta} \cdot \vec{E}, \quad (\text{II-25})$$

where

$$\frac{1}{\gamma^2} = 1 - \vec{\beta}^2. \quad (\text{II-26})$$

The momentum is $\vec{p} = \gamma m \vec{v} = \gamma m \vec{\beta} c$, its energy is γmc^2 , and the charge magnitude $e = |e|$. We have five equations and four unknowns x , y , z and γ .

Substituting the magnetic field from equation (II-2) into equations (II-24), (II-25) and (II-26) yields the following equations

$$\frac{d(\gamma \vec{\beta}_\perp)}{dt} = -\frac{e}{mc} [E(1 - \beta_z)(\cos \psi, -\sin \psi, 0) + \beta_z B(-\sin(k_0 z), \cos(k_0 z), 0)] \quad , \quad (\text{II-27})$$

$$\frac{d(\gamma \beta_z)}{dt} = -\frac{e}{mc} [E(\beta_x \cos \psi - \beta_y \sin \psi) + B(\beta_x \sin(k_0 z) - \beta_y \cos(k_0 z))] \quad , \quad (\text{II-28})$$

$$\frac{d(\gamma)}{dt} = -\frac{e}{mc} E[\beta_x \cos \psi - \beta_y \sin \psi], \quad (\text{II-29})$$

where $\vec{\beta}_\perp = \vec{\beta}_x + \vec{\beta}_y$ and $\psi = kz - \omega t + \phi$. There are more equations than unknowns, so we can ignore the β_z component.

The electrons are traveling near the speed of light along the z axis, so we can estimate that $\beta_z \approx 1$. This means that $E(1 - \beta_z) \ll B\beta_z$, and the first term of the transverse components of (II-22) can be ignored. Thus,

$$\frac{d(\gamma \vec{\beta}_\perp)}{dt} \cong -\frac{e}{mc} [\beta_z B(-\sin(k_0 z), \cos(k_0 z), 0)], \quad (\text{II-30})$$

Which implies that the static undulator field controls the transverse motion of the electron almost entirely. We

can integrate (II-30) by inspection, yielding the following results

$$\bar{\beta}_\perp = -\frac{K}{\gamma} [\cos(k_0 z), \sin(k_0 z), 0]. \quad (\text{II-31})$$

Substituting (II-31) into (II-29) yields

$$\dot{\gamma} = \frac{eKE}{\gamma mc} \cos(\zeta + \phi) \quad (\text{II-32})$$

where $\zeta + \phi = \psi + k_0 z = (k + k_0)z - \omega t + \phi$. From (II-31)

$$\beta_\perp^2 = \frac{K^2}{\gamma^2}, \quad (\text{II-33})$$

and substituting into to (II-26)

$$\frac{1}{\gamma^2} = 1 - (\bar{\beta})^2 = 1 - \beta_z^2 - \beta_\perp^2 = 1 - \beta_z^2 - \frac{K^2}{\gamma^2} \quad (\text{II-34})$$

so that

$$(1 + K^2) \frac{1}{\gamma^2} = 1 - \beta_z^2. \quad (\text{II-35})$$

Taking the time derivative of (II-35),

$$\frac{\dot{\gamma}}{\gamma} = \frac{\gamma^2 \beta_z \dot{\beta}_z}{1 + K^2} \quad (\text{II-36})$$

From the derivative of the electron phase, we have

$$\dot{\zeta} = (k + k_0)\dot{z} - \omega = (k + k_0)c\dot{\beta} - \omega, \quad (\text{II-37})$$

and

$$\ddot{\zeta} = (k + k_0)c\dot{\beta}_z, \quad (\text{II-38})$$

so that

$$\dot{\beta}_z = \frac{\ddot{\zeta}}{(k + k_0)c} . \quad (\text{II-39})$$

Substituting into (II-36), we get

$$\frac{\dot{\gamma}}{\gamma} = \frac{\gamma^2 \beta_z \dot{\beta}_z}{1 + K^2} = \frac{\gamma^2 \beta_z \ddot{\zeta}}{(1 + K^2)(k + k_0)c} . \quad (\text{II-40})$$

Now equating (II-32) and (II-40), we get

$$\frac{\gamma^2 \beta_z \ddot{\zeta}}{(1 + K^2)(k + k_0)c} = \frac{eE_0 K}{mc} \cos(\zeta + \phi) , \quad (\text{II-41})$$

and solving for $\ddot{\zeta}$, we have

$$\ddot{\zeta} = \frac{(1 + K^2)}{\gamma^2} \frac{(k + k_0)c}{\beta_z} \frac{eE_0 K}{\gamma^2 mc} \cos(\zeta + \phi) . \quad (\text{II-42})$$

Since $k \gg k_0$, we can use the approximation $(k + k_0) \approx k$. From

equation (II-6) $\omega_0 = ck_0 = ck(1 + K^2)/2\gamma^2$, and using $\beta_z \approx 1$,

equation (II-42) reduces to

$$\ddot{\zeta} = \frac{2\omega_0 eEK}{\gamma^2 mc} \cos(\zeta + \phi) \quad (\text{II-43})$$

Converting to dimensionless time with $dt = Ld\tau/c$, and defining the dimensionless optical field magnitude as

$$|a| = \frac{4\pi NeKLE}{\gamma^2 mc^2} , \quad (\text{II-44})$$

The pendulum equation becomes

$$\ddot{\zeta} = |a| \cos(\zeta + \phi) . \quad (\text{II-45})$$

The pendulum equation (II-45) is the same form for a linear undulator. However, for the linear undulator, the optical

field $|a|$ is modified by substituting $K[J_0(\xi) - J_1(\xi)]$ for K , where $\xi = K^2/2(1+K^2)$ and $J_0(\xi)$ and $J_1(\xi)$ are Bessel functions.

D. OPTICAL WAVE EQUATION

The pendulum equation describes how individual electrons are affected by the laser field. To describe how the laser field is affected by the beam of electrons, we next derive the optical wave equation. Begin with the inhomogeneous wave equation for the optical vector potential \bar{A} ,

$$\left[\bar{\nabla}^2 - \frac{1}{c^2} \frac{\partial^2}{\partial t^2} \right] \bar{A} = -\frac{4\pi}{c} \bar{J}_\perp, \quad (\text{II-46})$$

where

$$\bar{E}_s = -\frac{1}{c} \frac{\partial \bar{A}}{\partial t} = E[\cos \psi, -\sin \psi, 0], \quad (\text{II-47})$$

$$\bar{B}_s = \bar{\nabla} \times \bar{A} = [\sin \psi, \cos \psi, 0], \quad (\text{II-48})$$

$\psi = kz - \omega t + \phi$. When the amplitude and phase of the laser beam change slowly with time, we can write the vector potential in the form

$$\bar{A}(z, t) = \frac{c}{\omega} E(z, t) [\cos(\psi), -\sin(\psi), 0]. \quad (\text{II-49})$$

The form in equation (II-49) assumes that the electron beam is small compared to the waist of the optical mode, so that the transverse direction is not important. \bar{A} is dependent only on z and t . The spatial derivative is

$$\begin{aligned}
\frac{\partial^2 \bar{A}}{\partial z^2} = & \frac{1}{k} \frac{\partial E}{\partial z} \left[k + \frac{\partial \phi}{\partial z} \right] [\cos(\psi), -\sin(\psi), 0] + \\
& \frac{1}{k} \frac{\partial^2 E}{\partial z^2} [\sin(\psi), \cos(\psi), 0] + \\
& \frac{1}{k} \frac{\partial E}{\partial z} \left[k + \frac{\partial \phi}{\partial z} \right] [\cos(\psi), -\sin(\psi), 0] + \\
& \frac{E}{k} \frac{\partial^2 \phi}{\partial z^2} [\cos(\psi), -\sin(\psi), 0] + \\
& \frac{E}{k} \left[k + \frac{\partial \phi}{\partial z} \right]^2 [-\sin(\psi), -\cos(\psi), 0]
\end{aligned} \tag{II-50}$$

and the time derivative is

$$\begin{aligned}
\frac{\omega}{c} \frac{\partial^2 \bar{A}}{\partial t^2} = & \frac{\partial E}{\partial t} \left[\frac{\partial \phi}{\partial t} - \omega \right] [\cos(\psi), -\sin(\psi), 0] + \frac{\partial^2 E}{\partial t^2} [\sin(\psi), \cos(\psi), 0] \\
& + \frac{\partial E}{\partial t} \left[\frac{\partial \phi}{\partial t} - \omega \right] [\cos(\psi), -\sin(\psi), 0] + E \frac{\partial^2 \phi}{\partial t^2} [\cos(\psi), -\sin(\psi), 0] \\
& + E \left[\frac{\partial \phi}{\partial t} - \omega \right]^2 [-\sin(\psi), -\cos(\psi), 0] .
\end{aligned} \tag{II-51}$$

From the assumption that phase and amplitude varies slowly, $\partial E / \partial z \ll kE$, $\partial \phi / \partial z \ll k\phi$, $\partial E / \partial t \ll \omega E$, and $\partial \phi / \partial t \ll \omega \phi$. From these approximations, we find that

$$\begin{aligned}
\left[\bar{\nabla}^2 - \frac{1}{c^2} \frac{\partial^2}{\partial t^2} \right] \bar{A} \approx & 2 \left[\frac{\partial E}{\partial z} + \frac{1}{c} \frac{\partial E}{\partial t} \right] [\cos(\psi), \sin(\psi), 0] \\
& + 2E \left[\frac{\partial \phi}{\partial z} + \frac{1}{c} \frac{\partial \phi}{\partial t} \right] [-\sin(\psi), -\cos(\psi), 0] = -\frac{4\pi}{c} \bar{J}_\perp .
\end{aligned} \tag{II-52}$$

To further simplify, we use a coordinate transformation, where the position z moves along with the optical field at the speed of light c , so that $\tilde{z} = z + ct$. Also, we convert to dimensionless time, $\tau = ct/L$ to get

$$\left(\frac{\partial}{\partial z} + \frac{\partial}{c \partial \tau} \right) = \frac{\partial}{c \partial t} = \frac{\partial}{L \partial \tau}, \quad (\text{II-53})$$

and

$$2 \left[\frac{1}{L} \frac{\partial E}{\partial \tau} \right] [\cos(\psi), \sin(\psi), 0] + 2E \left[\frac{1}{L} \frac{\partial \phi}{\partial \tau} \right] [-\sin(\psi), -\cos(\psi), 0] \approx -\frac{4\pi}{c} \bar{J}_\perp. \quad (\text{II-54})$$

Each electron adds to the total current, so the current density contribution from the i^{th} electron is summed to get

$$\bar{J}_\perp = -ec \sum_i \bar{\beta}_\perp \delta^{(3)}(\vec{x} - \vec{r}_i) \quad (\text{II-55})$$

where the \vec{r}_i is the trajectory of the i^{th} electron and $\delta^{(3)}$ is a three dimensional Dirac Delta Function. Substituting, the transverse velocity $\bar{\beta}_\perp = -K / \gamma (\cos(k_0 z), \sin(k_0 z), 0)$ into the current gives

$$-\frac{4\pi}{c} \bar{J}_\perp \approx \sum_i -\frac{4\pi e K}{\gamma} [\cos(k_0 z), \sin(k_0 z)] \delta^{(3)}(\vec{x} - \vec{r}_i). \quad (\text{II-56})$$

Therefore, the wave equation is

$$\left[\frac{\partial E}{\partial \tau} \right] [\cos(\psi), \sin(\psi), 0] + E \left[\frac{\partial \phi}{\partial \tau} \right] [-\sin(\psi), -\cos(\psi), 0] = \sum_i -\frac{2\pi e K L}{\gamma} [\cos(k_0 z), \sin(k_0 z)] \delta^{(3)}(\vec{x} - \vec{r}_i) \quad (\text{II-57})$$

Both sides of (II-57) averaged over a volume element dV_c , which is smaller than the coherence volume, yet larger than a wavelength of the light. The current density over this small volume element is constant, so the summation over i electrons $\sum_i (-2\pi e K L / \gamma) [\cos(k_0 z), \sin(k_0 z)] \delta^{(3)}$ can be replaced

with a charge density ρ times the average of sample electrons in the beam, the average is symbolized by $\langle \rangle$. So now we have two uncoupled equations

$$\frac{\partial E}{\partial \tau} = -\frac{2\pi e \rho L K}{\gamma} \langle \cos(\zeta + \phi) \rangle \quad (\text{II-58})$$

$$\frac{\partial \phi}{\partial \tau} = \frac{2\pi e \rho L K}{\gamma} \langle \sin(\zeta + \phi) \rangle \quad (\text{II-59})$$

where $\psi + k_0 z = \zeta + \phi$. Defining the dimensionless current $j = 8\pi^2 e^2 \rho N K^2 L^2 / \gamma^3 m c^2$, and recalling the dimensionless optical field $|a| = 4\pi N e K L E / \gamma^2 m c$, the change in electric field amplitude becomes

$$\frac{\partial |a|}{\partial \tau} = \left| \dot{a} \right| = -j \langle \cos(\zeta + \phi) \rangle. \quad (\text{II-60})$$

Since the electric field is complex, then $a = |a|e^{i\phi}$, and we arrive at the optical wave equation

$$\dot{a} = -j \langle e^{-i\zeta} \rangle. \quad (\text{II-61})$$

Equation (II-61) is derived for a helical undulator. However the same form of the equation applies to a linear undulator provided K is replaced by $K[J_0(\xi) - J_1(\xi)]$.

E. GAIN MECHANISMS

For the FEL to be operational, there must be an increase in power of the optical field each pass through the undulator. There are two regions of optical gain: the low

gain region ($j \leq \pi$) and the high gain region ($j \gg \pi$). To understand the mechanisms behind gain we first develop the concept of an electron phase space plot.

1. Phase Space

The electron phase space is a plot of an electron's phase velocity, $v(\tau) = \dot{\zeta} = L[(k + k_0)\beta_z - k]$ and the electron phase $\zeta(t) = (k + k_0)z(t) + \omega t$. In the low gain case $\dot{a} \approx 0$, which means that equation (II-61) evolves slowly so that $|a|$ and ϕ are approximately constant. Multiplying both sides of the electron pendulum equation (II-45) by $\dot{\zeta}$ yields

$$\ddot{\zeta} \dot{\zeta} = |a| \cos(\zeta + \phi) \dot{\zeta} = \dot{v} v \quad , \quad (\text{II-62})$$

or

$$\dot{v} v - |a| \cos(\zeta + \phi) \dot{\zeta} = 0 \quad , \quad (\text{II-63})$$

so that

$$\frac{d}{d\tau} \left[\frac{v^2}{2} - |a| \sin(\zeta + \phi) \right] = 0. \quad (\text{II-64})$$

This means that $v^2 - 2|a| \sin(\zeta + \phi) = \text{constant}$, and

$$v^2 = v_0^2 - 2|a| [\sin(\zeta + \phi) - \sin(\zeta_0)]. \quad (\text{II-65})$$

Where $v_0 = v(0)$ and $\zeta_0 = \zeta(0)$ are the initial phase velocity and phases. Equation (II-65) is a statement of energy conservation in the dimensionless coordinates ζ and v . The

equation also identifies paths in the phase space, $v(\zeta)$, that describes the electron motion. In Figure II-2, several phase space paths are plotted. δ refers to taper and will be discussed in the next section.

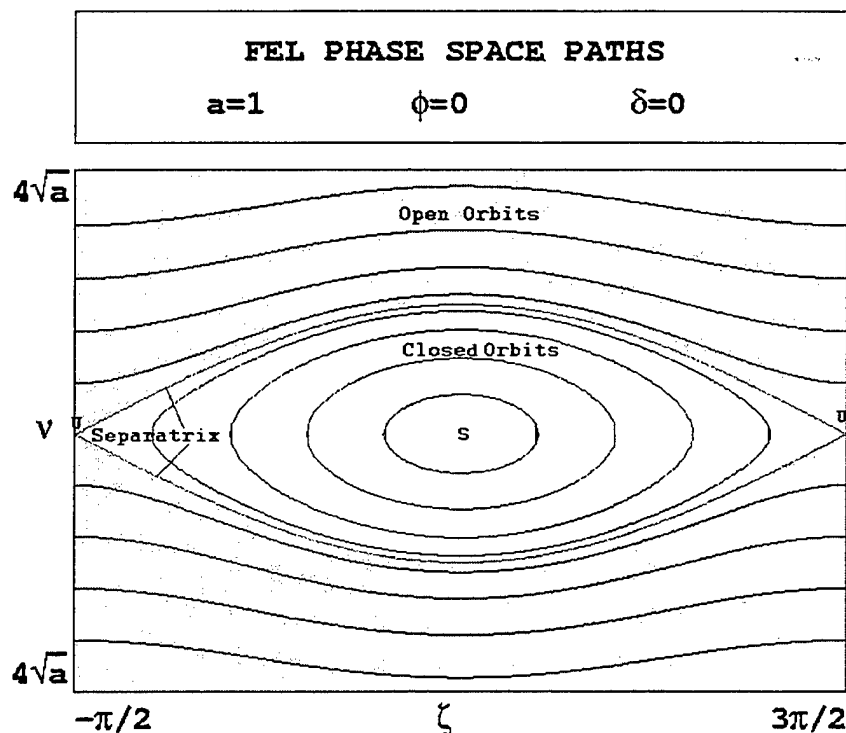


Figure II-2 Phase Space Diagram

2. Separatrix

Electrons stay on $v(\zeta)$ paths in the ζ - v plane. These paths are based upon the initial phase velocity v_0 and initial phase ζ_0 of the electron and the pendulum equation. This same equation describes an undamped, undriven pendulum where ζ is the tilt angle and v is the angular velocity. The

critical points for these paths occur at $v=0$ and $\zeta=\pi/2\pm\pi n$ where $n=1,2,3$. The stable fixed points occur when $\zeta=\pi/2\pm 2\pi n$. In Figure II-2 the stable fixed point is labeled with an "S". The unstable fixed points are at $v=0$ and $\zeta=3\pi/2\pm 2\pi n$. In Figure II-2, the unstable fixed points are labeled with a "U". At these fixed points, the electron remains stationary in phase space. At $(v,\zeta)=(\pi/2,0)$, the pendulum is hanging at the bottom of the arc. When $|v|>2|a|^{1/2}$, the pendulum has enough angular momentum to swing continually over the top around in a circle. In phase space, we can draw a separatrix which separates the lower closed orbits from the over-the-top open orbits. The equation for the separatrix is

$$v_s^2 = 2|a|[1 - \sin(\zeta_s + \phi)]. \quad (\text{II-66})$$

In Figure II-2, the separatrix separates the open orbits, shown as a gray area, from the closed orbits, shown as a white area.

3. Bunching

Consider a collection of electrons that are initially uniformly distributed in phase evolving along the undulator. The pendulum equation shows that for $-\pi/2 \leq \zeta \leq \pi/2$, $\ddot{\zeta} > 0$ and the electron phase accelerates, while for $\pi/2 \leq \zeta \leq 3\pi/2$, $\ddot{\zeta} < 0$ and the phase decelerates. The result is that the

electrons tend to bunch about $\pi/2$ as they evolve along the undulator.

4. Changes in Phase Velocity

From the definition of phase velocity $v(\tau) = L[(k + k_0)\beta_z - k]$, we find the change in beam energy due to a change in phase velocity. Taking the derivative of both sides near resonance where $v=0$, $k \gg k_0$ and $N=L/\lambda_0$, we get $\delta v \approx Lk\delta\beta_z \approx N\lambda_0 k\delta\beta_z$. From equation (II-6) and the resonance condition, $\lambda = \lambda_0(1 + K^2)/2\gamma^2$, we find that

$$\delta v \approx 4\pi N \frac{\delta\gamma}{\gamma} \approx 2\pi N \frac{\delta\lambda}{\lambda}. \quad (\text{II-67})$$

Thus, an increase in v results in an increase of the electron energy, γmc^2 , and the optical wavelength λ .

5. Gain Formula

Gain is defined as $\Delta P/P$, where ΔP is the change in optical power in one pass through the undulator, and P is the power at the beginning of the undulator. From (II-67) the average change in energy for an electron in the undulator is

$$\Delta\bar{\gamma}mc^2 \approx \gamma mc^2 (\langle v \rangle - v_0) / 4\pi N, \quad (\text{II-68})$$

where $\langle v \rangle$ is the average final energy. The number of electrons in a volume dV of the optical wave is given by $\rho F dV$ where ρ is the electron density and F is the filling factor. The filling factor F is the cross-sectional area of

the electron beam divided by the cross-sectional area of the light beam. The radiation energy in a volume dV is given by $2E^2 dV / 8\pi$ in cgs units. Invoking the definition of the dimensionless field a and the dimensionless current j , we arrive at

$$G = \frac{[\rho F dV] [\gamma m c^2 (\langle v \rangle - v_0) / 4\pi N]}{[2E^2 dV / 8\pi]} = \frac{2Fj}{a_0^2} \langle v_0 - v \rangle. \quad (\text{II-69})$$

6. Low Gain

For low gain, the optical field changes vary slowly so we can estimate that $\dot{a} \approx 0$ with the initial conditions $v(0)=v_0$, $a(0)=a_0$, and $\zeta(0)=\zeta_0$. From perturbation theory, we find that

$$v = v_0 + \frac{a_0^2}{v_0^2} [\sin(\zeta_0 + v_0 \tau) - \sin(\zeta_0)] + \frac{a_0^2}{v_0^3} \left[-\frac{1}{4} \cos(2\zeta_0 + 2v_0 \tau) - \cos(2\zeta_0) + \cos(2v_0 \tau) - \right] + \dots \quad (\text{II-70})$$

$$1 - v_0 \tau \sin(\zeta_0) \cos(\zeta_0 + v_0 \tau)$$

Taking take the time average of the phase velocity, we find

$$\langle v \rangle = v_0 + \frac{a_0^2}{v_0^3} [2 \cos(v_0 \tau) - 2 + v_0 \tau \sin(v_0 \tau)] + \dots \quad (\text{II-71})$$

The gain is therefore

$$G = \frac{2jF}{a_0^2} \langle v_0 - v \rangle = \frac{jF}{v_0^3} [2 - 2 \cos(v_0 \tau) - v_0 \tau \sin(v_0 \tau)]. \quad (\text{II-72})$$

7. High Gain

In the high gain regime the current is very large, $j \gg \pi$. Unlike the low gain regime, we cannot ignore the rapid evolution of the optical field over a single pass. Combining the expanded pendulum and optical equation and integrating over all the initial electron phases, $\int d\zeta_0$, we get

$$\ddot{a}(\tau) = \frac{ij}{2} \int d\tau' \tau' F(\tau') e^{-i\nu_0 \tau'} a(\tau - \tau') \quad (\text{II-73})$$

where $F(\tau') = \int dq f(q) e^{-iq\tau'}$ is the characteristic function of the distribution $f(q)$. $f(q)$ is the distribution of the initial electron phases $\nu_i = \nu_0 + q$ about ν_0 and $\int dq f(q) = 1$.

The low current gain formula can be obtained from this equation by considering a perfect beam where $f(q) = \delta(q)$ and $a(\tau - \tau') \approx a_0$, in which case a_0 can be moved outside the integrand. Further integration results in the low gain formula shown earlier.

To find the solution to equation (II-73), we need to consider a perfect beam with $F(\tau') = 1$ and a resonant optical field $\nu_0 = 0$. Then, taking two derivatives, we get

$$\ddot{a}(\tau) = \frac{ij}{2} a(\tau). \quad (\text{II-74})$$

It can be shown that the solution to (II-74) is

$$a(\tau) = \frac{a_0}{3} \left[e^{(j/2)^{1/3}(i+\sqrt{3})\tau/2} + e^{(j/2)^{1/3}(i-\sqrt{3})\tau/2} + e^{(j/2)^{1/3}\tau} \right] \quad (\text{II-75})$$

Since for high gain $j \gg \pi$ the dominate exponential terms are the fastest growing terms. The following approximations can be made for the optical field amplitude, phase and gain:

$$|a(\tau)| \approx \frac{a_0}{3} e^{(j/2)^{1/3}\sqrt{3}\tau/2}, \quad (\text{II-76})$$

$$\phi(\tau) \approx \left(\frac{j}{2} \right)^{1/3} \frac{\tau}{2}, \quad (\text{II-77})$$

$$G(\tau) \approx \frac{1}{9} \left[e^{(j/2)^{1/3}\sqrt{3}\tau} \right]. \quad (\text{II-78})$$

The gain grows exponentially along τ with a growth rate proportional to $j^{1/3}$.

F. BEAM QUALITY

Previously, when considering the interaction of the electron and optical pulse we assumed perfect injection. In reality there are errors involved. The two factors that have the most influence are electrons injected off axis at the initial position, y_0 , and electrons injected at an initial angle, θ_y . From Reference (2) the decrease in phase velocity is

$$\Delta \bar{v} = \frac{2\pi N}{1 + K^2} (K^2 k_0^2 y_0^2 + \gamma^2 \theta_y^2). \quad (\text{II-79})$$

The change in phase velocity from these errors is made more severe with more undulator periods N . A longer FEL is more sensitive to injection errors.

A measure of the quality of the electron beam is the emittance, $\epsilon_y = \bar{y}_0 \bar{\theta}_y$, where \bar{y}_0 is the rms initial position spread of electrons along y , and $\bar{\theta}_y$ is the rms initial angular spread of the electrons in the y direction. The beam can be focused to minimize either \bar{y}_0 or $\bar{\theta}_y$, however emittance ϵ_y remains fixed. The minimum change in phase velocity occurs when the beam is "matched" so that both terms in (II-79) contribute equally. Matching occurs when $Kk_0 y_0 \approx \gamma \theta_y$. For a matched beam $\Delta \bar{v} \approx 2\pi N_0 K k \epsilon_y / \gamma$.

To show the effects of beam quality we need to look at the FEL integral equation (II-73). The function $f(q)$ in equation (II-73) has a distribution based only on the initial distribution of the electrons as they enter the undulator. Two examples of distributions are those from the electron phase velocity and injection angle. The spread in phase velocity can be considered a Gaussian distribution about v_0 with a standard deviation of $\sigma_v = 4\pi N \Delta \bar{v} / \gamma$. The angular spread leads to an exponential distribution with a standard deviation given by $\sigma_\theta = 4\pi N \gamma^2 \bar{\theta}_y^2 / (1 + K^2)$. The distributions are

$$f_G(q) = \frac{e^{-q^2 / 2\sigma_G^2}}{\sqrt{2\pi}\sigma_G}, \quad (\text{II-80})$$

and

$$f_\theta(q) = \frac{e^{q / \sigma_\theta}}{\sigma_\theta}. \quad (\text{II-81})$$

The characteristic function for these two cases are

$$F_G(q) = e^{-q^2 \tau^2 / 2\sigma_G^2}, \quad (\text{II-82})$$

and

$$F_\theta(q) = \frac{1}{1 - i\sigma_\theta \tau} \quad (\text{II-83})$$

For perfect injection $\sigma_G=0$ and $\sigma_\theta=0$, we have $F(\tau)=1$. When the beam is not perfect the characteristic function $|F(\tau)|$ decays with a characteristic time $1/\sigma_G$ or $1/\sigma_\theta$. $F(\tau)$ depends on the shape of the function $f(q)$, and different distributions of $f(q)$ effect the FEL's ability to bunch.

G. SHORT PULSE EFFECTS

In the low gain FEL, the modes of light in the oscillator can develop independently. Since the electrons are relativistic, they travel to, but less than, the speed of light. At resonance, one wavelength of light passes over an electron as the electron travels through one undulator period. Over the total length of the undulator the electron slides behind the light by $N\lambda$, called the slip distance. In the transverse dimension, the optical mode is roughly the

radius of the optical beam which is $(N\lambda/\pi)^{1/2}$. These modes evolve as determined by the pendulum equation and wave equation.

In order to follow the evolution of the optical field, we must set up multiple sites in z along the complex wave envelope. The transformation to spatial modes, $a \rightarrow a(z)$, is the equivalent to the transformation to wave numbers, $a \rightarrow a(k)$. The longitudinal position on the z -axis Z is transformed to dimensionless parameters by dividing by the slippage distance $N\lambda$, therefore $z \rightarrow Z/N\lambda$. Throughout the remainder of this paper z is dimensionless parameter.

The length of the electron pulse l_e becomes the dimensionless parameter $\sigma_z = l_e/N\lambda$. The pendulum and wave equations of motion with slippage included become

$$\ddot{\zeta}_{z-\tau} = |a_z| \cos(\zeta_{z-\tau} + \phi_z) \quad (\text{II-84})$$

and

$$\dot{a}_z = -j_{z-\tau} \langle e^{-i\zeta_{z-\tau}} \rangle. \quad (\text{II-85})$$

The electron current is $j_z = 8\pi^2 e^2 \rho(z) N K^2 L^2 / \gamma^3 m c^2$, where the electron density, $\rho(z)$, is the density at the site z . A site in the electron beam interacts with and amplifies N optical wavelengths, while the optical wave passes over and attempts to bunch electrons in a slip distance along the electron beam.

Short pulses of spontaneous radiation drive a typical FEL oscillator. When the length of the electron pulse, l_e , is comparable to the slip distance, short pulse effects influence the interaction. As the electron and optical pulses pass over each other, the pendulum equation (II-85) sees a continually changing optical field, a_z , while the wave equation (II-86) sees a continually changing current density $j_{z-\tau}$ and bunching distribution $\langle e^{-i\zeta_z-\tau} \rangle$. In the resonator, the optical pulse bounces between two mirrors. The distance between the mirrors is S which is necessarily greater than the length of the undulator, L . The time interval for the light-pulse make one round trip is $2S/c$.

Desynchronism, d , is the difference between the arrival times of the electron and optical pulses at the beginning of the pass, again normalized by the slip distance $N\lambda$. If $d=0$ at $\tau=0$, the electron pulse arrives simultaneously with the light-pulse. Moving one of the mirrors slightly by ΔS changes d so that $d=-\Delta S/N\lambda$.

H. TAPER

1. Purpose of Taper

In a successful FEL design, the optical field will eventually saturate due to over-bunching of the electrons along the undulator, thereby changing the dynamics of the

electron interaction. As the electron loses energy to the optical field, the phase velocity moves off resonance by $\Delta v \approx 4\pi N \Delta \gamma / \gamma \approx -2\pi$. One way to extend saturation to higher powers is to taper the undulator field. Instead of a periodic sinusoidal magnetic field with constant amplitude, the amplitude of the field is either increased or decreased progressively along the length of the undulator. Either shortening the undulator period along the undulator, or changing the strength of the magnetic field along the undulator tapers the undulator. In either case, acceleration of the phase of the electron results.

This acceleration is denoted by δ , or the taper parameter, so that $\dot{v} = \delta$, and

$$\delta = -4\pi N \frac{K \Delta K}{1 + K^2}, \quad (\text{II-86})$$

where the undulator field is tapered by ΔK over the undulator length. The electron pendulum equation becomes

$$\ddot{\zeta} = \dot{v} = \delta + |a| \cos(\zeta + \phi). \quad (\text{II-87})$$

While the optical wave equation (II-86) remains unchanged.

2. Taper Phase Space

In the limit of low gain the phase space paths for the tapered undulator are given by

$$v = \left[v_0^2 - 2\delta(\zeta - \zeta_0) - 2|a|[\sin(\zeta + \phi) - \sin(\zeta_0 + \phi)] \right]^{\frac{1}{2}} \quad (\text{II-88})$$

The stable fixed point for both positive ($\delta > 0$) and negative taper ($\delta < 0$) in phase space is at

$$(\zeta, \nu) = (\cos^{-1}(-\delta/|a|) - \phi, 0) \quad (\text{II-89})$$

The unstable fixed points depends upon the direction of the taper. The unstable fixed point for $\delta > 0$ in phase-space is located at

$$(\zeta, \nu) = (2\pi - \cos^{-1}(-\delta/|a|) - \phi, 0) \quad (\text{II-90})$$

and for $\delta < 0$ it is at

$$(\zeta, \nu) = (-\cos^{-1}(-\delta/|a|) - \phi, 0). \quad (\text{II-91})$$

The formula for the separatrix is

$$\nu_s^2 = 2\delta(\zeta_s - \zeta_0) + 2|a|[\sin(\zeta_s + \phi) - \sin(\zeta_0 + \phi)], \quad (\text{II-92})$$

where $\zeta_0 = 2\pi - \cos^{-1}(-\delta/a)$ for $\delta > 0$ and $\zeta_0 = -\cos^{-1}(-\delta/a)$ for $\delta < 0$.

Figure II-3 shows phase space plots for negative and positive tapers. "U" refers to the unstable fixed point, and "S" refers to the stable fixed point.

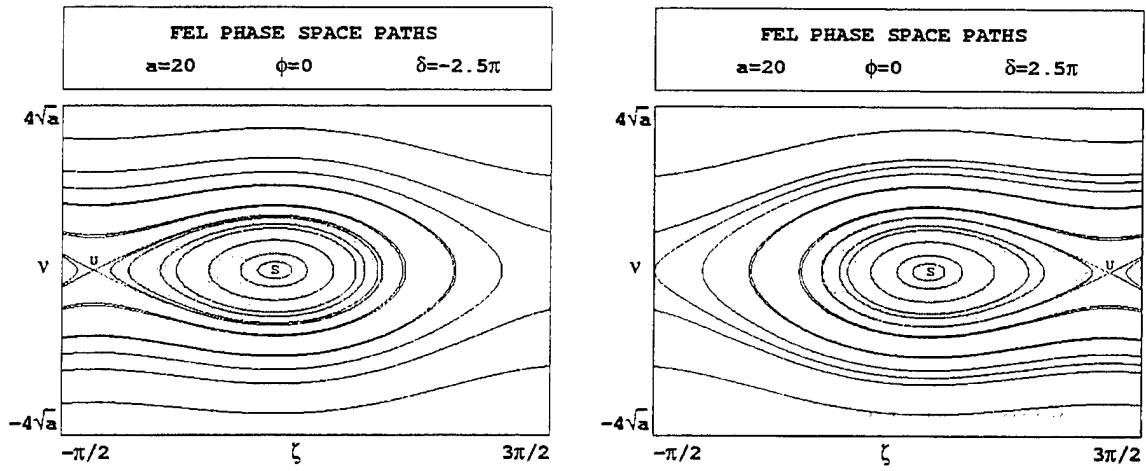


Figure II-3 Phase Space Plots for Negative and Positive Taper

III. TAPER SEPARATRIX HEIGHT

To find the height of the separatrix for the tapered undulator it is convenient to make a few variable changes and assume that there is no initial phase (which only shifts the separatrix along x) $\zeta = x$, $v = y$, $\phi = 0$, and $\zeta_0 = x_0$. Hence, equation (II-95) becomes

$$y^2 = 2\delta(x - x_0) + 2|a|(\sin x - \sin x_0) \quad (\text{III-1})$$

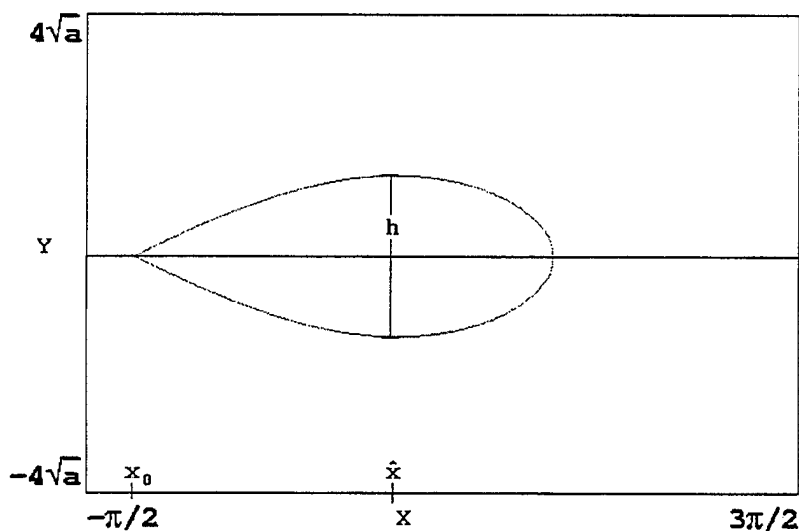


Figure III-1 Separatrix for negative taper with $q=0.4$

Figure III-1 shows the separatrix for a taper $\delta=-2.5$ and an optical field $a_0=20$. The height of interest is the maximum height labeled h in Figure III-1. To find the maximum value, we need to take the derivative of equation (III-1) which gives

$$2yy' = 2\delta + 2|a|\cos x, \quad (\text{III-2})$$

where $y' = dy/dx$, and set the slope y' equal to zero

$$y' = \frac{\delta + |a| \cos x}{y} = 0. \quad (\text{III-3})$$

The maximum value for x can be denoted as \hat{x} and is given by

$$\delta + |a| \cos \hat{x} = 0 \quad \text{or} \quad \hat{x} = \cos^{-1}(-q), \quad (\text{III-4})$$

where $q = \delta/|a|$. Note that q is restricted to values between 1 and -1.

A. POSITIVE TAPER

For $\delta > 0$, $x_0 = 2\pi - \cos^{-1}(-q)$ and substituting \hat{x} for x gives

$$y^2 = 2\delta [\cos^{-1}(-q) - (2\pi - \cos^{-1}(-q))] + 2|a| [\sin(\cos^{-1}(-q)) - \sin(2\pi - \cos^{-1}(-q))] \quad (\text{III-5})$$

Using the identity $\sin(2\pi - x) = -\sin(x)$ we can simplify equation (III-5) to get

$$y^2 = 2\delta [2 \cos^{-1}(-q) - 2\pi] + 2|a| [2 \sin(\cos^{-1}(-q))] . \quad (\text{III-6})$$

Factoring out $|a|$ we have

$$y^2 = 4|a| [q(\cos^{-1}(-q) - \pi) + \sin(\cos^{-1}(-q))] . \quad (\text{III-7})$$

Using the identities $\cos^{-1}(-x) - \pi = -\cos^{-1}(x)$ and

$\sin(\cos^{-1}(-q)) = \sqrt{1 - q^2}$, we can consolidate equation (III-7)

to get

$$y^2 = 4|a| [-q \cos^{-1}(q) + \sqrt{1 - q^2}] . \quad (\text{III-8})$$

Taking the square root of both sides, we get the maximum value of y to be

$$y = \left(2\sqrt{|a|} \left[-q \cos^{-1}(q) + \sqrt{1 - q^2} \right] \right)^{\frac{1}{2}}. \quad (\text{III-9})$$

The height of the separatrix, h is twice the value of y therefore,

$$h = 4\sqrt{|a|} \left[-q \cos^{-1}(q) + \sqrt{1 - q^2} \right]^{\frac{1}{2}}. \quad (\text{III-10})$$

B. NEGATIVE TAPER

For negative q , $x_0 = -\cos^{-1}(-q)$. Therefore equation (III-1) becomes

$$y^2 = 2\delta \left[\cos^{-1}(-q) - (-\cos^{-1}(-q)) \right] + 2|a| \left[\sin(\cos^{-1}(-q)) - \sin(-\cos^{-1}(-q)) \right]. \quad (\text{III-11})$$

Utilizing the identity $\sin(-x) = -\sin(x)$, it becomes

$$y^2 = 4\delta \left[\cos^{-1}(-q) \right] + 2|a| \left[-\sin(\cos^{-1}(-q)) - \sin(\cos^{-1}(-q)) \right] \quad (\text{III-12})$$

Consolidating and factoring out $|a|$ gives

$$y^2 = 4|a| \left[q(\cos^{-1}(-q)) + \sin(\cos^{-1}(-q)) \right]. \quad (\text{III-13})$$

Take the square root of both sides gives

$$y = 2\sqrt{|a|} \left[q \cos^{-1}(-q) + \sqrt{1 - q^2} \right]^{\frac{1}{2}} \quad (\text{III-14})$$

and then the height is

$$h = 4\sqrt{|a|} \left[q \cos^{-1}(-q) + \sqrt{1 - q^2} \right]^{\frac{1}{2}} \quad (\text{III-15})$$

Equations (III-10) and (III-15) are equivalent with the $|q|$.

Therefore we can say for all values of q

$$h = 4\sqrt{|a|} \left[-|q| \cos^{-1}(|q|) + \sqrt{1 - q^2} \right]^{\frac{1}{2}} \quad (\text{III-16})$$

C. POSTIVE AND NEGATIVE TAPER

Since the separatrix height for the non-tapered case ($\delta=0$) is

$$h = 4\sqrt{|a|} \left[-|q| \cos^{-1}(|q|) + \sqrt{1 - q^2} \right]^{\frac{1}{2}} \quad (\text{III-17})$$

Figure III-2 shows a graph of equation (III-18).

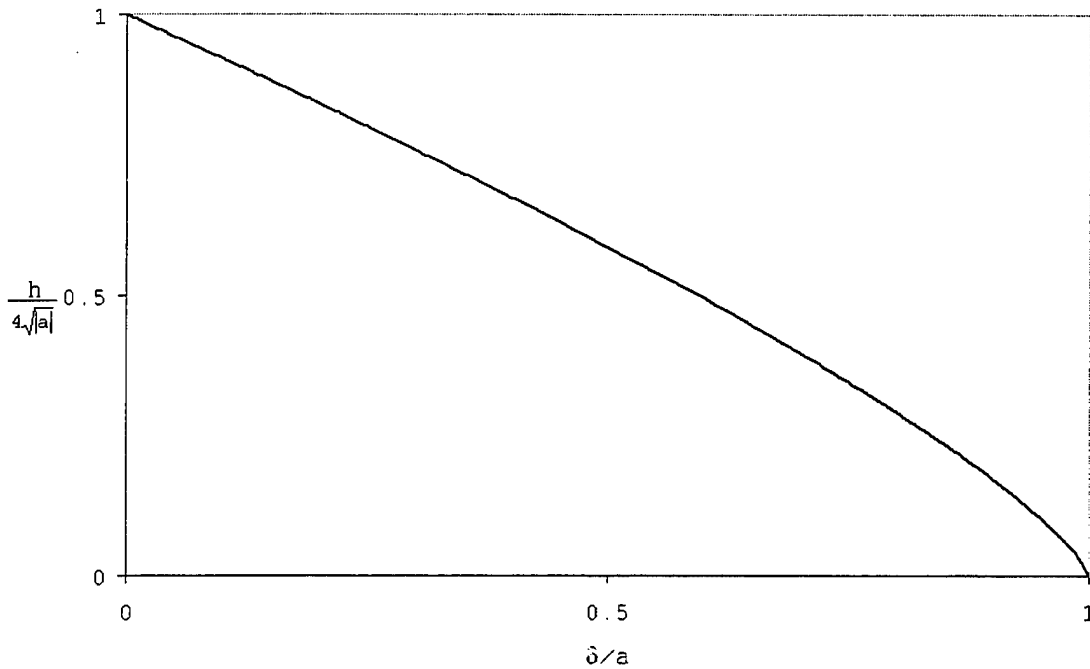


Figure III-2 Change in Separatrix Height δ/a

D. LINEAR APPROXIMATION

A Taylor expansion inside the brackets of equation (III-18) and using the expansion of arccosine

$$\cos^{-1}(q) = \frac{\pi}{2} - q + \dots \quad (\text{III-18})$$

gives

$$h = 4\sqrt{|a|} \left[-q \left(\frac{\pi}{2} - q \right) + 1 - \frac{1}{2} q^2 \right]^{\frac{1}{2}}. \quad (\text{III-19})$$

which simplifies to

$$h = 4\sqrt{|a|} \left[1 - \frac{\pi}{2} q + \frac{1}{2} q^2 \right]^{\frac{1}{2}} \quad (\text{III-20})$$

$$h = 4\sqrt{|a|} \left(1 - \frac{\pi}{4} q \right) = 4\sqrt{|a|} \left(1 - 0.785 \frac{\delta}{a} \right) \quad (\text{III-21})$$

From equation (III-21) it can be shown that, as $\delta \rightarrow 0$ the separatrix height $h \rightarrow 4\sqrt{|a|}$, or the size becomes the same as the untapered case. As the optical field $a \rightarrow \infty$ and the height $h \rightarrow 4\sqrt{|a|}$ the same as $\delta=0$. As the optical field becomes zero $a \rightarrow 0$ then the height $h \rightarrow 0$.

THIS PAGE INTENTIONALLY LEFT BLANK

IV. PARAMETERS FOR USE IN SIMPLE MODEL OF A HIGH GAIN FEL

To develop a simple model for a high gain FEL we need to first take a close look at the parameters that dominate the electron interaction with the optical field in the high gain regime. Table IV-1 is a table of several proposed and well-documented high gain FELs.

	Units	LCLS	TESLA	ELF85	ELF86	ELF87	MIT
KE	MeV	1500	35000	3.3	3.5	3.5	2.3
I	amps	3400	5000	500	850	1000	930
λ	cm	1.5×10^{-8}	1×10^{-8}	0.76	0.72	0.175	0.125
L	m	100	60	3	3	4	1.5
j	-	27200	35000	3300	5000	5600	3800
σ_x	-	0.45	0.003	0.045	0.04	0.12	0.16
a_0	-	0	0	12	14	0.34	0
λ_o	cm	3	5	9.8	9.8	9.8	3.14
N	-	3300	1200	30	30	40	48
N_β	-	0.3	0.4	11	11	5.7	2.3
σ_G	-	8.4	3.7	12	12	32	3.6
l_e	cm	0.008	20	450	1498	300	900
$N\lambda$	cm	3×10^{-5}	2×10^{-5}	23	22	7	6
Slip	-	186	1000	19	68	42	6,000
w_{ox}	cm	0.002	0.006	5	5	1.6	0.8
w_{oy}	cm	0.002	0.006	1.5	1.5	1.5	0.8
r_e	cm	0.003	.0018	0.4	0.3	0.6/ 1.2	0.4
ϵ	cm-rad	0.00015	0.0003	0.37	0.07	0.07	0.16
F	-	1	1	0.026	0.024	0.24	0.28

Table IV-1 Table of High Gain FEL Parameters

The following chapter is a description and analysis of each FEL in order to characterize them with our simple model.

A. DESCRIPTION OF LCLS AT SLAC

The Linac Coherent Light Source (LCLS) proposal is to use the last kilometer of Stanford Linear Accelerator Center (SLAC) to build a FEL able to achieve a 1.5 Å x-ray wavelength. An electron gun will inject an electron bunch that will be accelerated along the last kilometer of the SLAC accelerator to 14.35 GeV energy with a peak current of 3400 A. The normalized emittance is ϵ_N of 1.5 mm-rad. After the undulator, the electron beam will be dumped. The accelerator is tunable from 14.3 to 4.5 GeV which corresponds to x-ray wavelengths of 1.5-15 Å. The electron beam particle density is $\rho=2.5 \times 10^{16} \text{ cm}^{-3}$ in a beam radius of $r_e=30\mu$. The undulator will be a linearly polarized with a length of $L=112 \text{ m}$, period $\lambda_0=3.0 \text{ cm}$, number of periods $N=3328$, peak magnetic field strength $B=1.32\text{T}$ for a resultant undulator parameter of $K=2.6$, and a dimensionless current of $j=27,000$.

The FEL will be a single-pass amplifier starting from noise or spontaneous emission; a process called Stimulated Amplification from Spontaneous Emission (SASE). Due to the lack of mirrors at this wavelength, numerous proposals are

being investigated to guide the light once it leaves the FEL.

B. TESLA FEL AT DESY

The Deutsches Elektronen-Synchrotron (DESY) in Hamburg, Germany, is also planning to develop an x-ray FEL using the TeV Energy Superconducting Linear Accelerator (TESLA). The electron beam will be supplied by two 16 km long superconducting linear accelerators which were initially designed to collide electrons and positrons.

The specifications for the TESLA FEL are still under consideration and the project is being planned in conjunction with the LCLS with a later timeline. Many parameters will be based on experiments conducted in preparation for LCLS. The projections are based on beam energy of 25GeV and a peak current of 5kA.

C. ANALYSIS OF SLAC AND TESLA PARAMETERS

1. Wavelength

The purpose of these two lasers is to create a source of high power, coherent, hard x-rays at a 1 Å wavelength for numerous experimental uses. The lack of normal incidence optics at this wavelength creates many unique problems. Only grazing-incidence optics are possible, and they are still under development. The limited optics precludes the use of

an oscillator configuration and requires the FEL to operate as a single pass amplifier.

2. Reducing j

The dimensionless current j for both x-ray lasers is a large number. There are several factors, which lower the effective j for actual use in our simulations.

a) *Filling Factor*

In a typical FEL, the radius of the electron beam is smaller than that the optical mode. The filling factor is the cross sectional area of the electron beam divided by the cross sectional area of the optical beam. For LCLS and TESLA the cross sectional area of the electron beam is comparable to the cross sectional area of the optical beam, so $F \approx 1$. For LCLS, the radius of the electron beam r_e is about $0.03 \text{ mm} = 30 \text{ } \mu\text{m}$ so the normalized pulse width $\sigma_x \approx 0.45$. The radius of the optical field is approximately $w_0 \approx 0.02 \text{ m} = 2 \text{ } \mu\text{m}$.

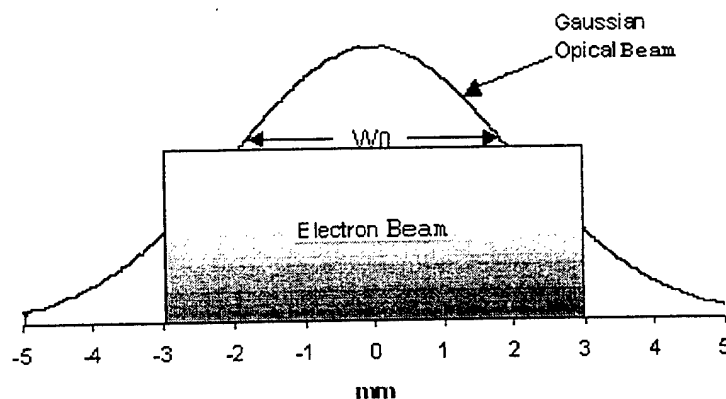


Figure IV-1 Gaussian X-ray Beam and Top-Hat Electron Beam

b) Betatron Oscillation

The number of electron betatron oscillations along the undulator in the x-ray FELs is small. The number of betatron oscillations along the undulator is inversely proportional to the energy of the electron beam. If there were a large number of betatron oscillations, then the average amount of time electron beam spend within the optical field is of little concern. Betatron oscillations cause the electrons to pass from the outside of the optical mode, where the fields are weak to the center of the mode, where the fields are strong. In order to account for the reduced bunching drive of the electrons due to betatron oscillations, due to the dimensionless current j is decreased by half.

3. Rayleigh Length

The waist size of the x-ray beam is very small with a $w_0=20 \text{ } \mu\text{m}$ radius. A small Rayleigh waist means a small Rayleigh length and large diffraction pattern a large distance away. The x-ray beam diffracts away from the electron beam contributing to reduced coupling. The Rayleigh length, $z_0 = \pi w_0^2 / \lambda$, for the LCLS this is approximately 30m, about one-third the length of the undulator. In a high-gain FEL such as LCLS the gain is exponential along the undulator. For LCLS, the gain in a Rayleigh length is about 100m as shown in Figure IV-2.

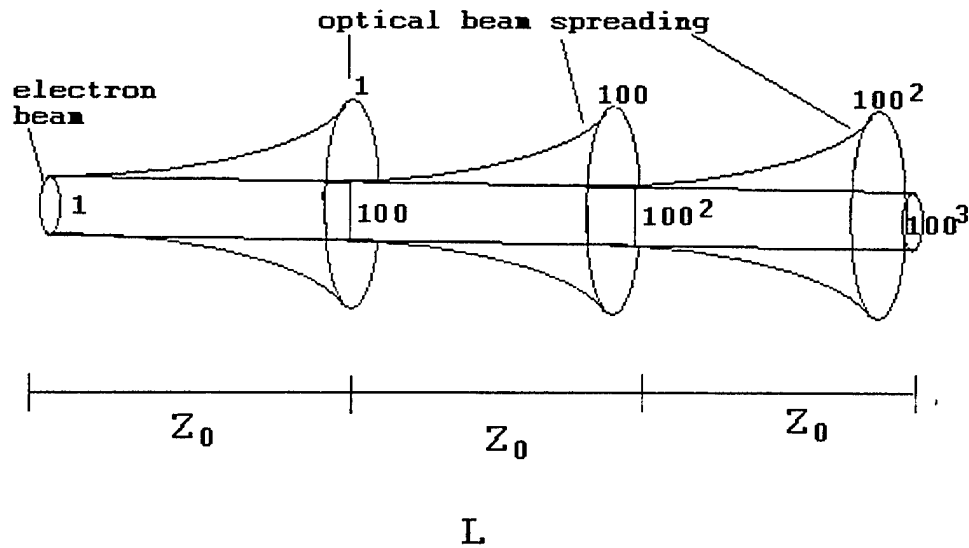


Figure IV-2 Discrete comparison of gain versus diffraction

To illustrate the reduced role of diffraction of the x-ray beam, divide the undulator into three discrete pieces. At the beginning of the undulator the optical power is taken to be 1 as shown in Figure IV-2 on the left. In one Rayleigh length, z_0 , along the length of the undulator, the gain is 100, but only within the region of the electron beam. The power in the center is 100, while the x-ray beam outside the electron beam has had no gain and remains power 1. The strength of the diffracted x-ray beam is only 1% of the power of the x-ray beam in the center. In the second Rayleigh length, the x-ray within the electron beam region has been amplified another factor of 100. The power in the center x-ray beam after two Rayleigh lengths is 100^2 . The power of the diffracted beam was amplified to 100 in the

first Rayleigh length and remains 100. Again this only 1% of amplified x-ray beam within the electron beam region. In the third length, the power at the end of the undulator has become 100^3 , while the diffracted light has only power of 100^2 . The power of the diffracted region is again only 1% of the power of the beam in the center at the end of the undulator.

In reality this is a continuous process along the undulator. But, just as for this discrete example, the continuous gain within the central area of the electron beam far out-weighs the gain at the edges of the electron beam. To account for this reduction in coupling, the value of j can be reduced by half, so that considering betatron motion and diffraction the final value is $j \approx 6700$. This is comparable to the other long wavelength FELs in Table IV-1.

4. Emittance

The emittance for the high gain FEL can be extremely important. The x-ray field growth is exponential with an e-folding time of $\tau_j \approx 2 / (j / 2)^{1/3} \sqrt{3} \approx 0.15$ for $j=5000$. For LSCS the emittance of $\sigma_\theta=0.7$, leads to a e-folding decay time of $\tau_\sigma \approx 1 / \sigma_\theta \approx 1.4$. Since the decay time caused by emittance is greater than the growth e-folding time driven by the electron beam, $\tau_\sigma \approx 1.4 > \tau_j \approx 0.1$. The net growth rate of the x-ray beam is significantly reduced along the undulator.

5. Slip

The electron pulse length is about 186 time longer than the slip distance $N\lambda$. The extremely short x-ray wavelength makes the slippage distance very small and short pulse effects are non-existent. Each part of the x-ray pulse experiences gain, which is proportional to the local density of electrons.

6. Initial Optical Field

Since no other laser can radiate near x-ray wavelengths, the x-ray FEL must seed itself. The initial x-ray field a_0 for an x-ray laser is necessarily zero, and the laser depends on the SASE (stimulated amplification of spontaneous emission) to begin. A simple simulation model is to start with a very small initial optical field that is representative of the spontaneous emission created in the beginning section of the undulator. In the first portion of the undulator, the model assumes that an initial optical field starts from random fluctuations in the electron beam density. The x-ray mode in SASE is known to be linear, starting from random noise, and growing through mode competition to the desired wavelength. Since the field growth in the beginning of the undulator is linear, instead of the exponential gain seen later along the undulator, a slightly longer undulator is required.

D. ELECTRON LASER FACILITY (ELF)

The Electron Laser Facility (ELF) is an offshoot of the Experimental Test Accelerator (ETA) located at Lawrence Livermore National Laboratory. The ELF was built to utilize the electron beam accelerated by ETA. In each year, 1985, 1986 and 1987 a paper was published updating that years experiments at ELF (references 4,5, and 6).. The main components of the laser remain essentially the same with several modifications from year to year. Here, the three phases of the ELF are referred to as ELF85, ELF86, ELF87. ELF85 had beam energy of 3.3 MeV and ELF86 and ELF87 had a beam energy of 3.5 MeV. ELF85 and ELF86 used a 3m long undulator which was extended in ELF87 to 4 meters. The undulator for all three is composed of specially shaped solenoids with a peak magnetic field of 5 kG. The wiggler period remained $\lambda_0=9.8$ cm for all three. The number of periods was $N=30$ and $N=40$ respectively. The peak current initially was 500 A for ELF85, then increased to 850 A for ELF86, and finally to 1000 A for ELF87. The wavelengths produced were $\lambda=0.76$ cm, 0.72 cm, and 0.175 cm. For each experiment, the optical field was contained in a 2.9 cm by 9.8 cm rectangular waveguide and the FELs were operated as single pass amplifiers.

E. ELF85

ELF85 has a dimensionless current $j=3300$. The dimensionless beam size σ_x is 0.045, and the initial optical field of $a_0=12$ was produced by a 60kW pulsed magnetron.

1. Electron Beam to Optical Field Ratio the Filling Factor

A sketch of the cross section of electron beam and optical mode is shown in Figure IV-3 and the filling factor is about $F=0.03$.

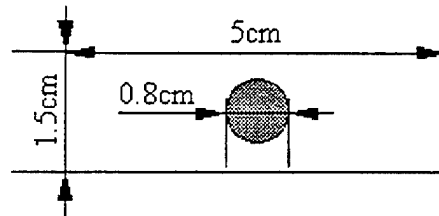


Figure IV-3 ELF 85 optical field(white), electron beam(gray) diagram

The electron beam is small enough so that electrons see only the peak of the optical beam. There are a large number of betatron oscillations along the undulator, unlike LCLS, but the electrons continue to see the peak optical field. The betatron oscillations increase little effect, since they remain within the optical field. There is some radiation in the harmonics due to the oscillation, but not enough to be significant.

2. Slip

The electron pulse is 20 slippage distances in length for ELF85. This is much smaller than for the LCLS, but still much larger than 1. Since the slip is larger than 1, short-pulse effects can still be neglected.

3. Emittance

The emittance for the beam was quite large $\epsilon=0.37$ cm-rad. This large emittance, assuming a matched beam, means a $\sigma_\theta=22$, and therefore a characteristic decay time of $\tau_\sigma=1/\sigma_\theta=0.045$. Gain degradation due to the emittance is quite significant.

F. ELF 86

The major difference between the ELF85 and ELF86 is the modification in the Experimental Test Accelerator (ETA) to use a field emission cathode. This increases the peak current and makes the pulse longer and the emittance smaller. The undulator dimensions remained the same.

1. Electron Beam to Optical Field Ratio, the Filling Factor

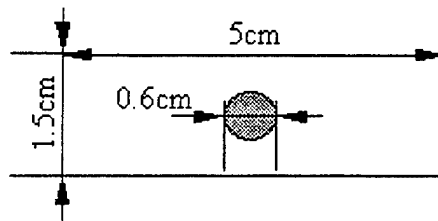


Figure IV-4 ELF 86 optical field, electron beam diagram

The ratio of the electron beam area to the optical beam area decreased slightly giving a filling factor $F=0.024$, as seen in Figure IV-4. The electron pulse length remained at 20 slippage distances with minimal short pulse effects. The dimensionless beam size σ_x remained nearly the same due to a slightly smaller optical wavelength 0.72 cm. The dimensionless current increased to $j=5000$. The input optical field is provided by a 100kW, 35GHz magnetron giving $a_0=14$.

The emittance was significantly reduced to $\epsilon=0.07$ cm-rad. The overall increase in current and better beam quality has increase the power output from 80 MW for ELF85 to 180MW for ELF86 and the efficiency increased from $\eta=5\%$ to $\eta=6\%$.

G. ELF87

A major change in ELF87 was the use of a high-current induction linac. This linac provided a beam energy of 3.5

MeV and a peak current of 1 kA. The dimensionless current $j=1000$ and the undulator was also extended to $L=4$ m.

Another major change was the shape of the electron pulse. The beam length cross section was oval as seen in Figure IV-5. However, this beam shape has little effect on the model.

The shift in the optical wavelength to $\lambda=0.175$ cm causes the optical mode to become much smaller. The ratio of electron beam area to optical mode area is much smaller. A process called optical guiding also causes the optical mode to remain small.

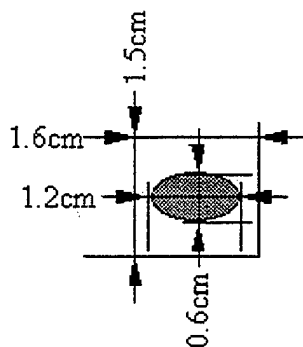


Figure IV-5ELF 87 optical field, electron beam diagram

The net effect is a larger filling factor, $F=0.24$, and more interaction between the light and the electron pulse.

H. MIT FEL

The MIT FEL is operated by the Department of Physics and Research Laboratory of Electronics, Massachusetts

Institute of Technology. This FEL was designed to operate at millimeter and sub-millimeter wavelengths. The MIT FEL has not been studied as closely, since it has lower gain than ELF. The most significant difference between this laser and the ELF laser is the undulator. The MIT laser uses a helical undulator.

1. Natural Focusing

An advantage of the helical undulator is the natural focusing of the electron beam. The magnetic field is always pushing the electrons toward the center of the beam. For an x-ray FEL, any added benefit from natural focusing could result in a significant increase in gain.

2. SASE

The other significant feature of the MIT laser is the SASE startup at long wavelengths. From its operation, it can be seen that SASE occurs within about the first 20 undulator periods. After the first 20 periods, the FEL field growth becomes exponential and can be simulated using a small initial optical field a_0 .

3. Electron Beam

A multielectron gun with a Pulserad 110A accelerator creates the electron beam. The beam is of relatively low kinetic energy, 2.3 MeV, with a peak current of 930 amps. The pulse length is 7200 times the slippage distance, so

that the light pulse interacts with the electrons along the entire length of the undulator.

I. CONCLUSION

In careful study of these FEL's, one can discern which parameters have the most influence on the growth rate and FEL interaction. A simulation model can often be simplified by concentrating on those parameters which create the large growth rate or decays, and ignoring those which have no discernible effect on the electron/optical field interaction. The parameters developed in this chapter can be used in a simple model. This is left for further study.

THIS PAGE INTENTIONALLY LEFT BLANK

V. DARMSTADT FEL

The next section is an analysis of the Darmstadt FEL utilizing computer simulations. The Darmstadt FEL is a medium gain laser and operates between $\lambda=6.6$ and $7.8\mu\text{m}$ wavelength, with electron beam energies between 32 and 29 MeV. It is driven by the S-DALINAC, a re-circulating electron linac using superconducting acceleration cavities, which allow for a continuous wave electron beam.

A. DARMSTADT PARAMETERS

The parameters for the Darmstadt FEL are shown in Table V-1. The primary use for the Darmstadt FEL is to provide infrared light for medical research. Most of the experiments involve medical uses such as ablation of biological tissue.

Electron Energy-KE	31 MeV
Peak Current-I	2.7 A
Electron Pulse Length- l_e	$600\mu\text{m}$
Number of Periods-N	80
Undulator period- λ_0	32mm
Undulator Parameter-K	0.78
Dimensionless current-j	1.6
Energy Spread- $\Delta E/E$	0.0023
Q-factor	110

Table V-1 Darmstadt parameters

B. BEAM SIZE EFFECTS ON GAIN

Initially the parameter values obtained for the Darmstadt FEL were not properly understood. The electron beam radius was given at the end of the undulator, and it was mistaken to be the radius at the center of the undulator. After several communications and some analysis, the discrepancy was discovered. As a result of angular spreading along the undulator the beam radius was 0.2mm at the waist, and a little less than 1mm at the end of the undulator. For an electron beam with Darmstadt's parameters and an electron beam waist radius $r_e=1\text{mm}$, the angular distribution would be $\sigma_\theta=7.3$. In the time it took to discover the error, an analysis of the influence of angular spread on gain was conducted. Despite not having any relevance to the Darmstadt FEL, the analysis was interesting and may have future relevance. Therefore the results are included here. The analysis below was conducted assuming an electron beam waist radius of 1mm.

1. Theoretical Background

An angular distribution of $\sigma_\theta=7.3$ is significant enough to degrade the gain of an FEL. A large electron beam radius means that there are a significant number of the electrons which are injected into the undulator that are off-set from the axis of propagation and at an angle with respect to that

axis. The larger the diameter, the more electrons that are injected off center and at larger angles. The electrons on the outer portion of the beam experience a larger magnetic field. These outer electrons are "wiggled" harder and therefore travel on a slightly longer path. As a result of the longer path, the electron slows down in the longitudinal direction with respect to an electron in the center of the beam. The spread in longitudinal velocities creates a spread in phase velocity. A spread in phase velocity then results in a reduction in gain.

The same argument can be used for electrons that are injected at an angle with the axis. An electron injected at an angle moves toward (or away from) the more intense magnetic field off axis. The electron is pushed back to the center harder than the other electrons and travels a longer distance. The longer distance means a greater spread in phase velocity and less gain.

2. Method of Analysis

In order to determine the effect of beam size on the gain, the effect of value of σ_0 on the gain is analyzed. The gain for each σ_0 must be calculated at the value of desynchronism giving maximum gain. For each σ_0 , there is a different desynchronism value d for which gain is a maximum. The amount of time to run enough simulations to determine the maximum gains for each σ_0 would have been prohibitive.

Gain versus desynchronism curves were plotted for $\sigma_0=7.3$ and $\sigma_0=3$, as shown in Figure V-1. In order to use this information to determine how the maximum d depends on σ_0 , linear interpolation was used. Assume a linear relationship between the maximum desynchronism d and σ_0 using the form $d = m\sigma_0 + b$ for a straight line. The maximum gain for each value of σ_0 can be estimated in subsequent simulations. Maximum gain was found for $\sigma_0=7.3$ at $d=0.003$, and for $\sigma_0=3$ at $d=0.0025$. After a small amount of algebra we find that $m=-0.00058$ and $b=0.0066$. To test the validity of this estimation, $\sigma_0=5$ was estimated to be a maximum at $d=0.0037$. A series of simulations shows that in fact, the maximum occurred at 0.0036; in good agreement with the interpolated formula. In Figure V-1 it can be seen that there is a flat plateau about the maximum of the curve, so our approximation for the maximum is accurate enough. In

Figure V-2 the gain found for each σ_0 , at the maximum d determined by the interpolation formula above, is plotted. A value of $\sigma_0=0$ means perfect injection, no deviation in either angle or position. The actual beam radius $r_e=0.2\text{mm}$ corresponds to $\sigma_0=0.3$ which is nearly perfect. The gain for $\sigma_0=0.5$ is about 3% less than for perfect injection which is an insignificant reduction.

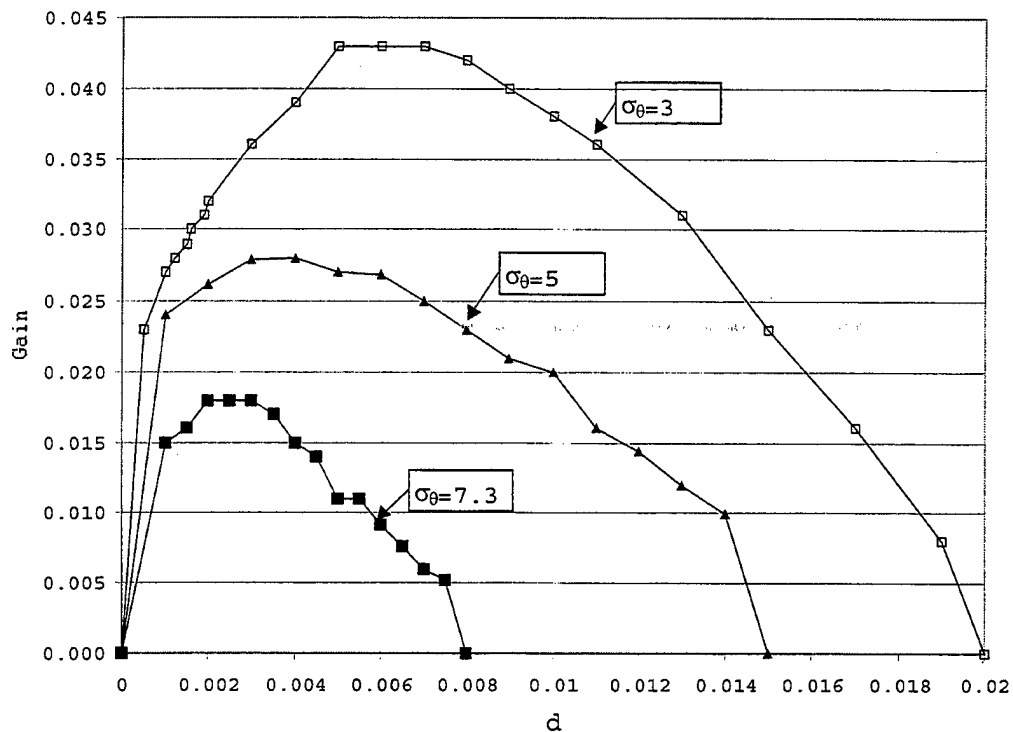


Figure V-1 Gain Versus Desynchronism

On the other hand, the original value of $\sigma_\theta=7.3$ results in a 77% decrease in gain which is not negligible. In fact, it would mean the Darmstadt FEL would not work.

From Figure V-2 the effects of an angular or radial spread on the reduction of Darmstadt gain can be straightforwardly determined.

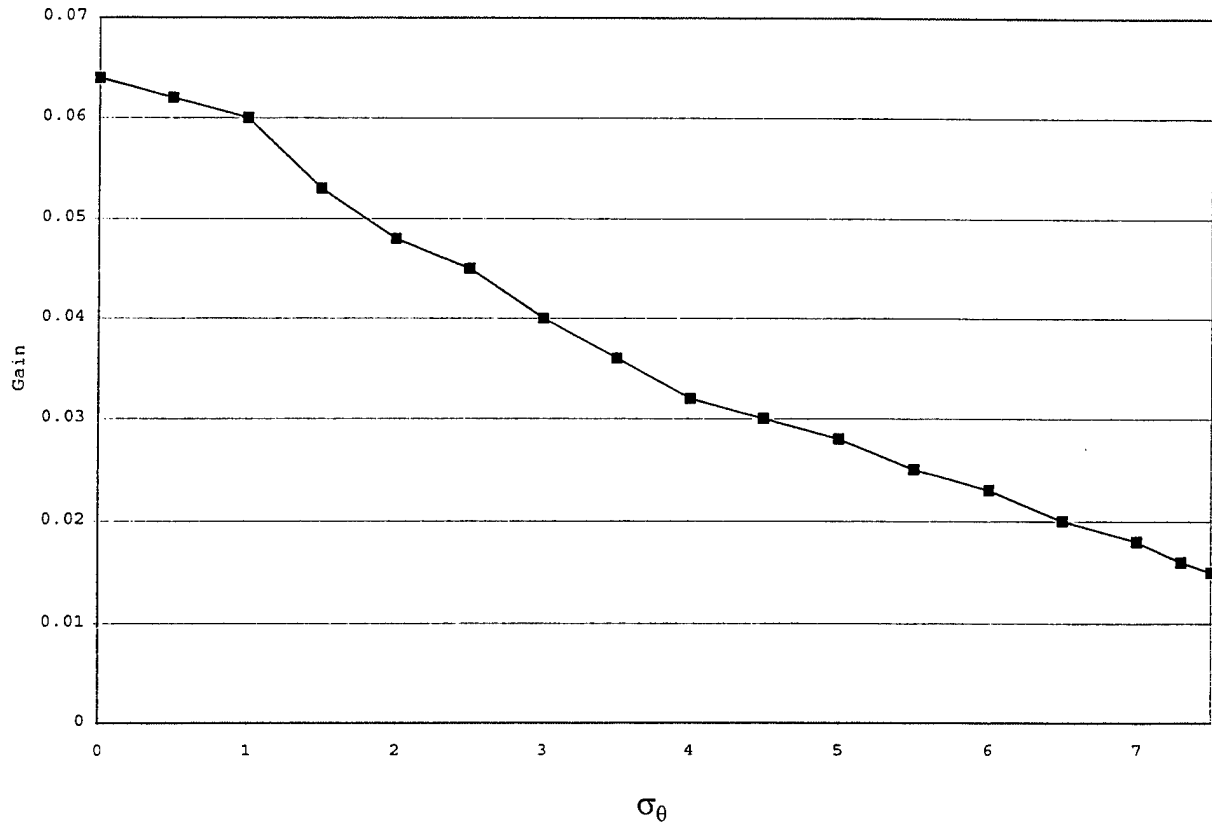


Figure V-2 σ_θ versus Gain

The final power P versus desynchronism d curves for $\sigma_\theta=7.3$ and $\sigma_\theta=3$ were plotted, as seen in Figure V-3. The final power in strong fields at saturation peaks at small values of d where gain is small, and extends out to larger values of d .

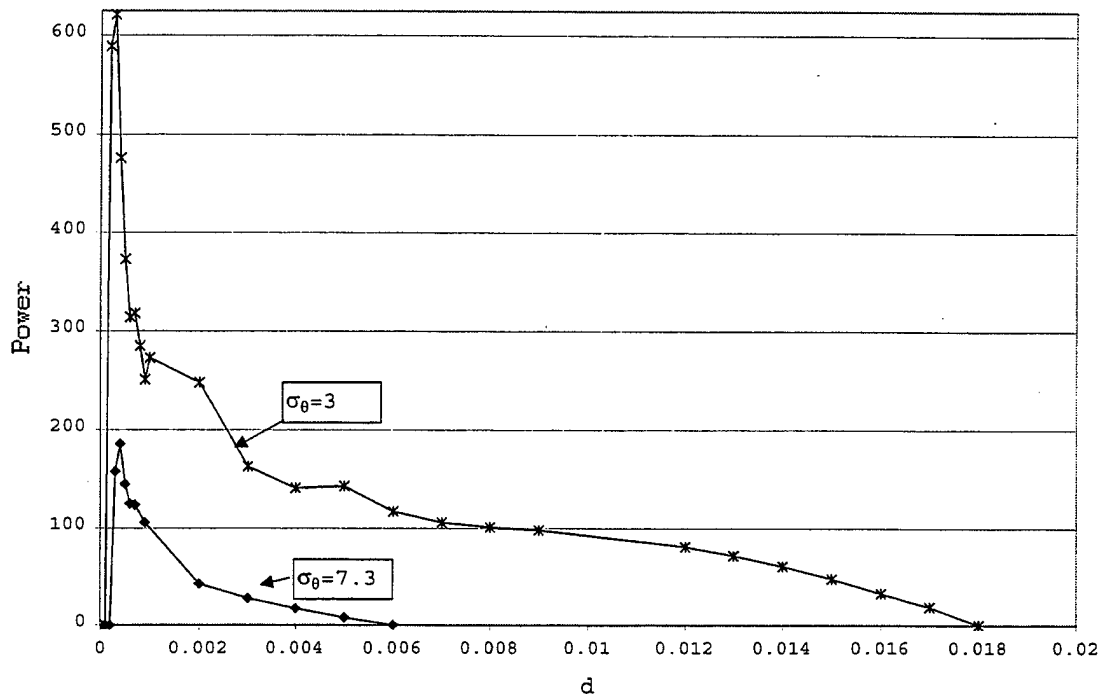


Figure V-3 Power Versus Desynchronism

C. TAPER EFFECTS

Using the actual Darmstadt FEL electron beam radius of $r_e=0.2\text{mm}$, and the parameters from Table V-1, the power versus desynchronism graphs for several tapers were determined. The following positive and negative tapers were analyzed: $\delta=-5.4\pi$, -2.5π , -0.63π , 0 , 1.3π , 2.5π , and 5.4π .

1. Compiled Data

Figure V-4 and Figure V-5 are 3-D graphs that depict power (on the vertical axis) as a function of both taper δ

and desynchronism \bar{d} . The two figures contain the same data but presented from different points of view.

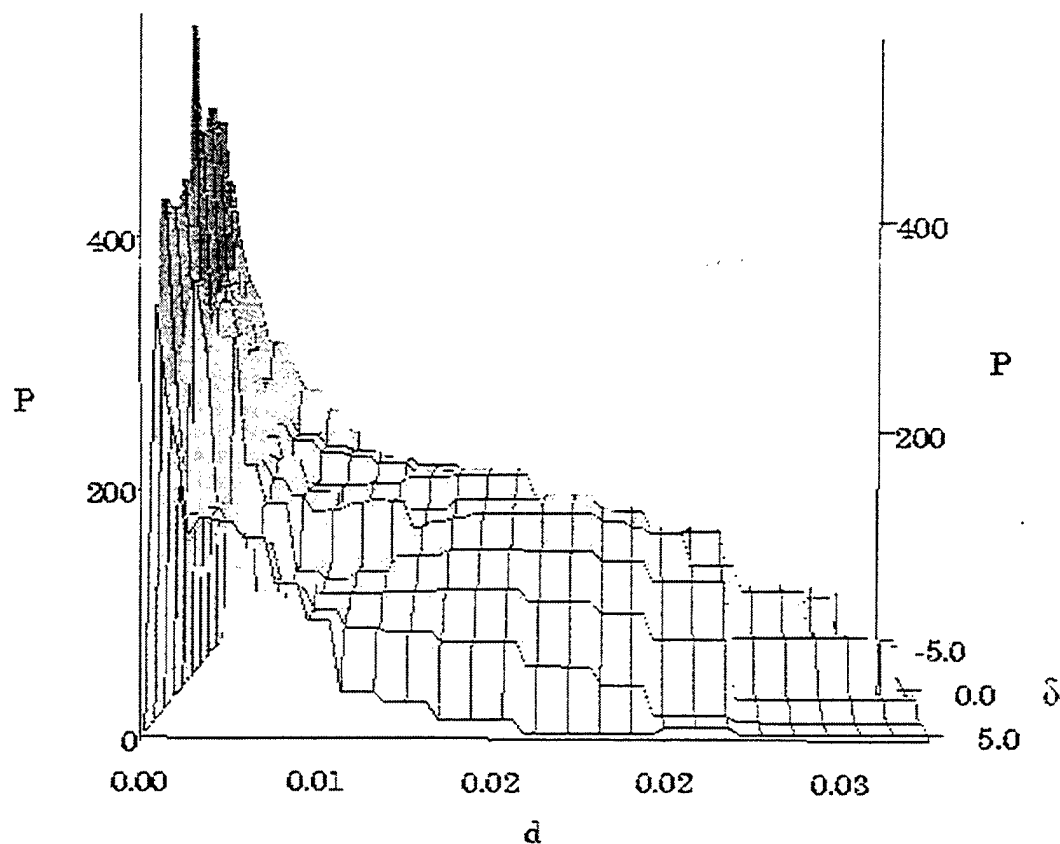


Figure V-4 3-D Plot of Power Versus, d , and δ (Positive View)

The power versus d curves $P(d)$ for each value of taper δ have similar structures. When $\bar{d}=0$, there is no power output at any δ . At approximately $\bar{d}=0.008$, the output power is maximum for each taper δ . The desynchronisms in the range $0 < d < 0.008$ do not produce any power for any taper.

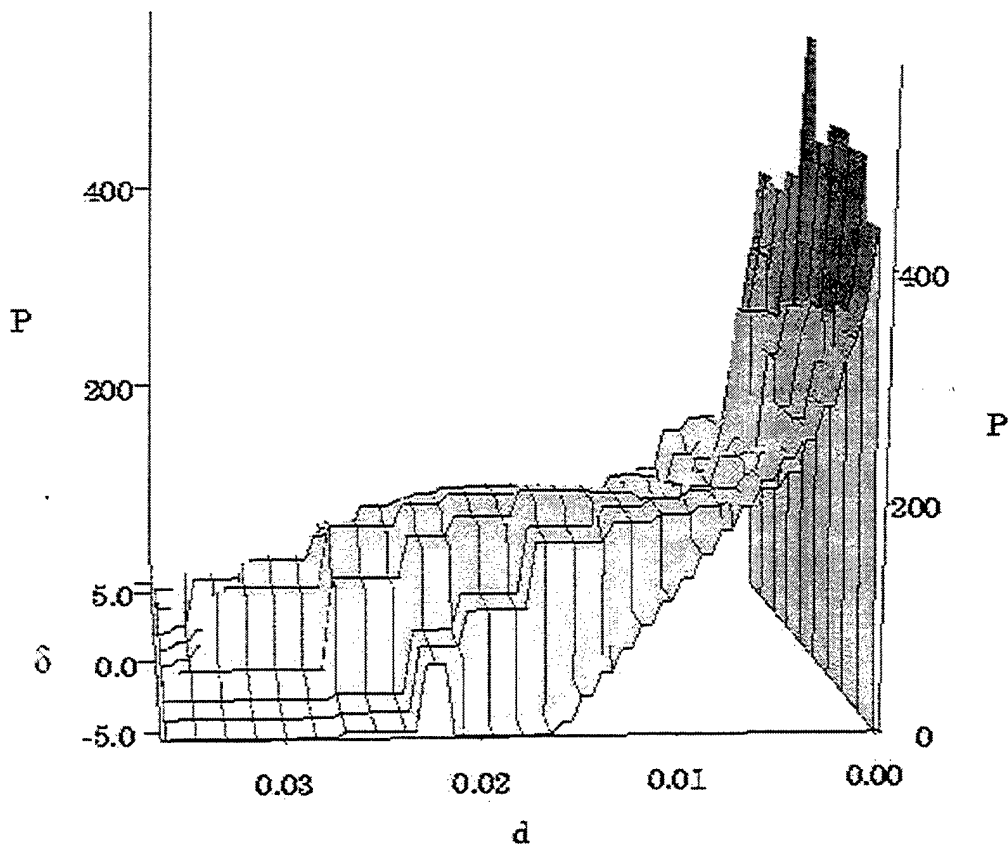


Figure V-5 3-D Plot of Power, d , and δ (Negative View)

The sharp rise in power and high peak power is typical of many FELs operating in this parameter regime. The largest peak power occurs at $\delta=0$.

A high quality factor Q means there are small optical losses per pass through the undulator. These losses include mirror loss and mirror transparency where optical power is removed for the end user. A high Q leads to sharper features in the desynchronism curves and to other important features explained in the next section.

2. Untapered Power Curve Analysis

To show more detail of the data in Figure V-4 and Figure V-5, Figure V-6 and Figure V-9 show power versus desynchronism with no taper $\delta=0$ and the highest value of negative taper $\delta=-5.4\pi$.

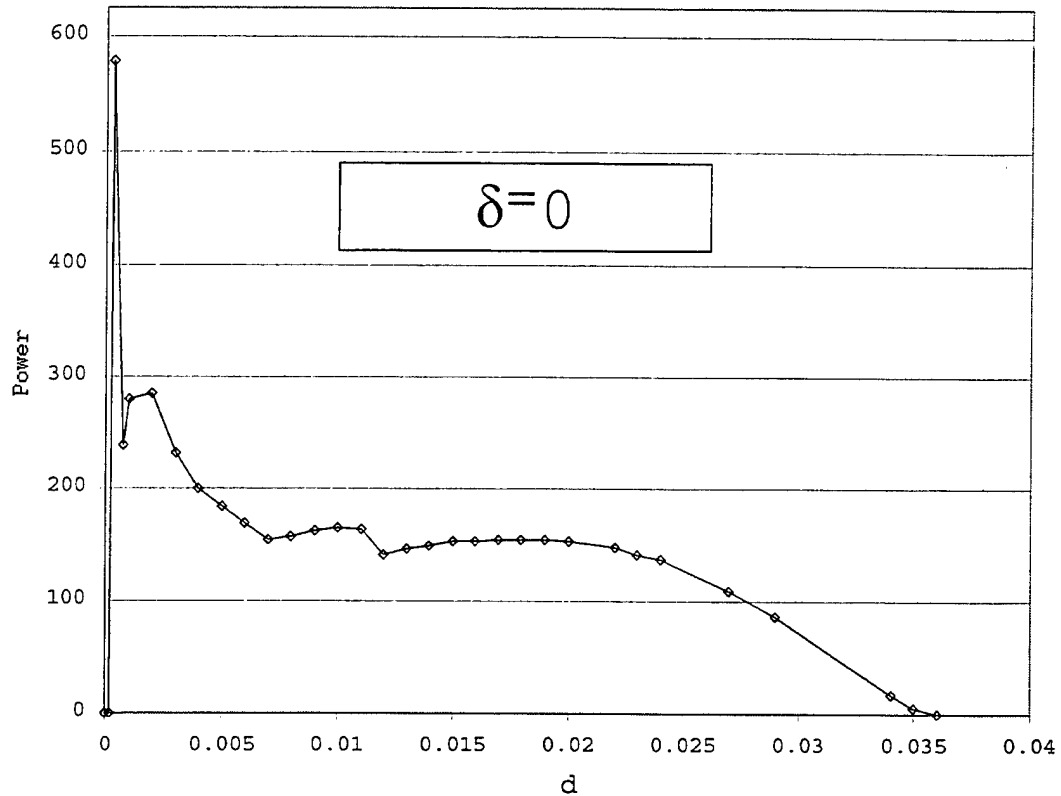


Figure V-6 P Versus Desynchronism $\delta=0$

In Figure V-6, the FEL exhibits limit-cycle behavior for desynchronisms between $d=0.0008$ and $d=0.011$ (ref (2)), and thus is not stable. Since the power levels are not stable the power in this region is an average of the power oscillations.

3. Simulation

Figure V-7 is the output from a single simulation run for the Darmstadt FEL. The input variables for this run are displayed in the top square. There are nine output windows displayed below the input window.

The top-left window shows the dimensionless optical field amplitude $|a(z)|$ at the end of $n=6000$ passes. The middle-left window shows the evolution of the field amplitude after at each pass $|a(z,n)|$, in this case for $n=6000$ passes. The lighter the color, the higher the amplitude, as is the case for each middle window. In the bottom-left window, the parabolic electron pulse $j(z-\tau)$ is plotted for reference at the beginning and end of the undulator; their separation shows the slippage along the undulator.

The bottom-center window plots for reference the weak-field gain spectrum as a function of phase velocity, v . The middle-center window shows the optical power evolution $P(v,n)$ as a function of phase velocity v at each pass n . The

top-center window show the final optical power spectrum $P(v)$ at the end of $n=6000$ passes.

The bottom-right window shows the total optical power evolution $P(n)$ as a function of the pass number n . The center-right window shows the evolution of the electron distribution in phase velocity $f(v,n)$ as a function of phase velocity and number of passes n . The upper-right window displays the final electron phase velocity distribution $f(v,6000)$ at the end of $n=6000$ passes.

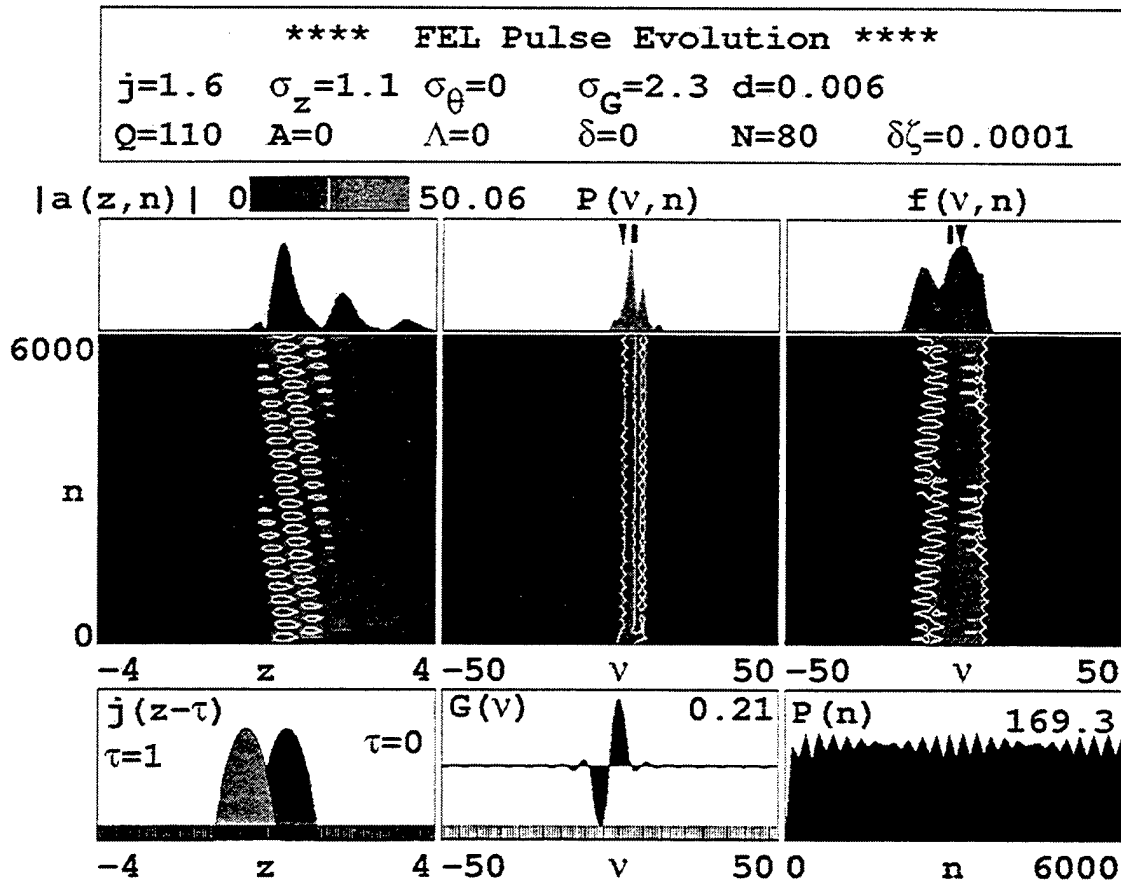


Figure V-7 Trapped Particle Instability

4. Limit-Cycle Behavior in the Untapered case

In the untapered undulator, the trapped-particle instability occurs for small values of desynchronism at $d=0.012$. In strong optical fields, electrons become trapped in the deep potential wells in phase space. These trapped electrons oscillate and radiate into side-bands off the main wavelength of the optical field. In the center window of Figure V-7, the side-bands off the main peak can be seen. Due to the power in the side-bands, limit-cycle behavior is present in the total power $P(n)$, and can be seen in the output power shown in the lower right hand window. The output power oscillates between two power levels as the FEL oscillates between two frequencies. The trapped particle instability does not always cause limit cycle behavior. In Figure V-8, the power exhibits chaotic output.

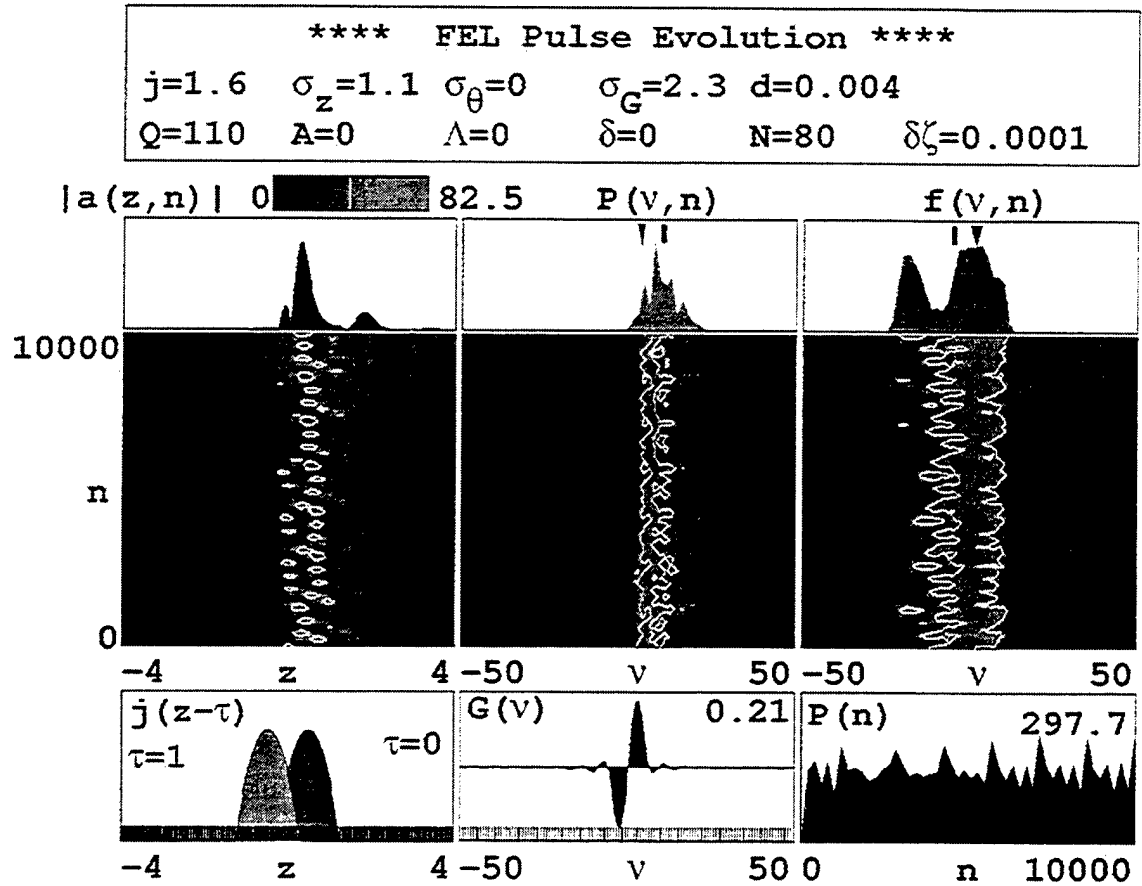


Figure V-8 Chaotic Power Output

5. Limit-Cycle Behavior in the Negative Tapered Case

Figure V-9 is the desynchronism curve $P(d)$ for the case of negative taper, $\delta=-5.4\pi$. For this taper $\delta=-5.4\pi$, limit cycle behavior never occurred, or was so small that it was not noticeable.

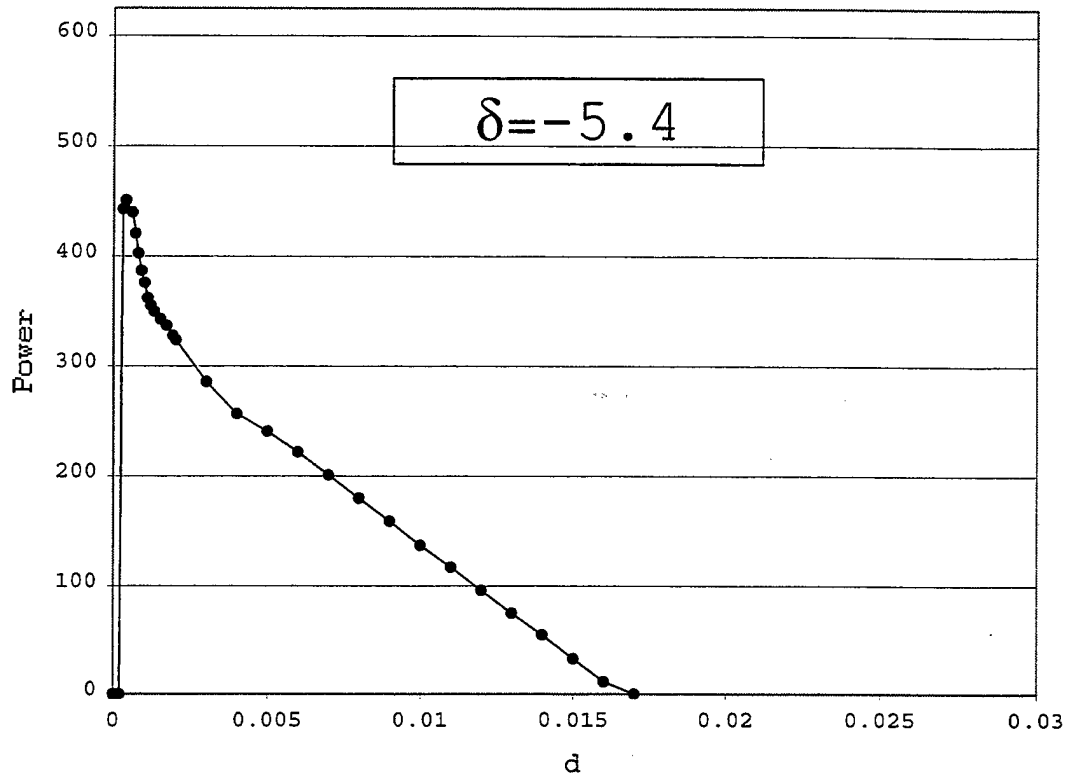


Figure V-9 P versus d $\delta=-5.4$

In Figure V-10, at the specific desynchronism $d=0.005$ and negative taper $\delta=-5.4$ we see there are no trapped particles. Above a certain value for d , $d=0.004$, the trapped particle instabilities do not occur. This results in smooth power output with no side bands around the optical wavelength as seen in the center window. The overall effect is a lower power output overall but provides for cleaner output power. This may be important for some applications where a narrow spectrum is important. For other applications more power may be important.

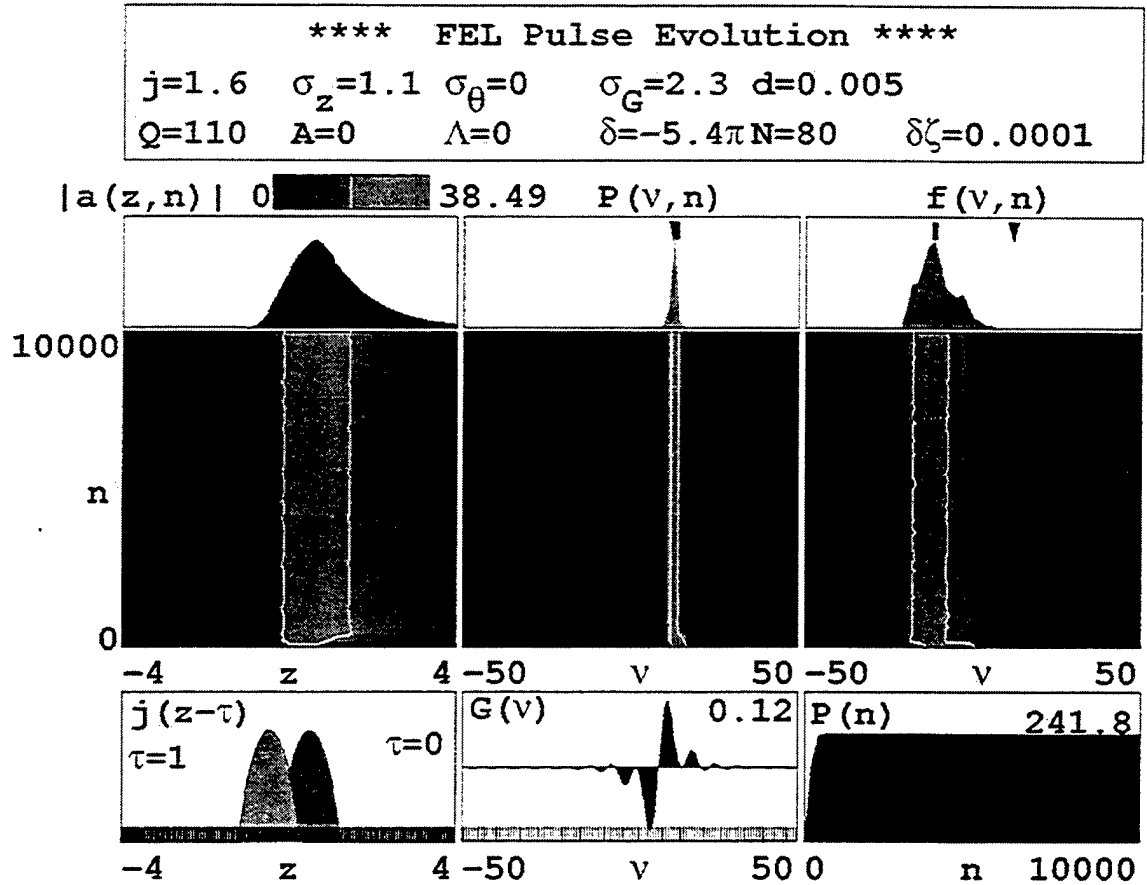


Figure V-10 No Trapped Particles

In Figure V-11, the effects of the trapped particle instability can be seen in the left and center windows. There is no limit cycle behavior as is seen from the steady power $P(n)$ window in the bottom right-hand window. In every taper studied, there were values of d for which the trapped particle instability occurred but no limit cycles.

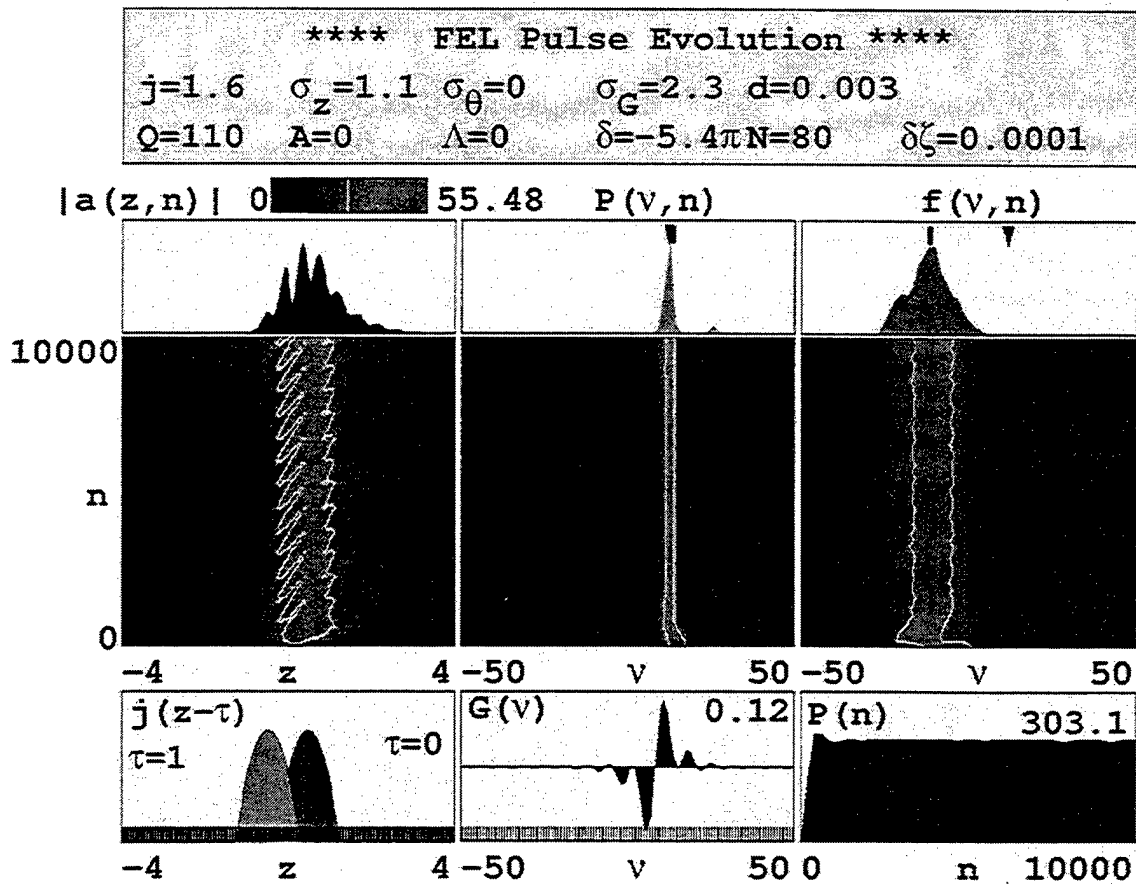


Figure V-11 Trapped Particles with Stable Power

D. CONCLUSION

The data collected from simulations of the Darmstadt FEL describe how decreasing electron beam quality would decrease that observed gain. Also simulations showed that there are regions of operation where limit-cycle behavior and chaos may be expected to occur in the experiment. It was also observed that the trapped-particle instability may occur without the presence of limit-cycles.

THIS PAGE INTENTIONALLY LEFT BLANK

LIST OF REFERENCES

1. W.B. Colson, *Laser Handbook*, Vol. 6, Chapter 5, North-Holland, 1990.
2. W.B. Colson, "Theory of High Gain Free Electron Lasers", *Nuclear Instruments and Methods in Physics Research A393*, 82-85, 1997.
3. J.H. Park and W.B. Colson, "A Simple Model of the LLNL ELF FEL Amplifier", *Nuclear Instruments and Methods in Physics Research A304*, 641, 1991.
4. Basics of Free-Electron Laser, Fundamenteel Onderzoek der Materie Institute for Plasma Physics (1999, December). Retrieved November 16, 2000, from the World Wide Web: <http://ns2.rijnh.nl/n4/n2/FELbasics.htm>
5. H. Nuhn and J. Rossbach, "LINAC-based Short Wavelength FELs: The ultimate X-ray source-the x-ray laser", *Synchrotron Radiation News*, Vol. 13 no. 1 2000.
6. T.J. Orzechowski, A.C.Anderson, W.M. Fawley, D. Prosnitz, E.T. Scharlemann, S. Yarema, D Hopkins, A.C. Paul, A.m. Sessler, and J. Wurtele, "Microwave Radiation from a High-Gain Free-Electron Laser Amplifier" *Physical Review Letters*, volume 54 number 9, 4 March 1985.
7. T.J. Orzechowski, A.C.Anderson, W.M. Fawley, D. Prosnitz, E.T. Scharlemann, S. Yarema, D Hopkins, A.C. Paul, A.m. Sessler, and J. Wurtele, "High Gain and High Extraction Efficiency from a Free Electron Laser Amplifier Operating in the Millimeter Wave Regime" *Nuclear Instruments and Methods in Physics Research A205*,144-149, 1986.
8. A.L. Throop, T.J. Orzechowski, B.R.Anderson, F.W. Chambers, J.C. Clark, W.M. Fawley, R.A. Jong, A.C. Paul, D. Prosnitz, E.T. Scharlemann, R.D. Stever, G.a. Westenskow, S.M. Yarema, K. Halback, D.B. Hopkins, and A.M. Sessler, "Experimental Characteristics of a High-Gain Free-Electron Laser Amplifier Operating at 8-mm and 2-mm wavelengths" preseneted at AIAA 19th Fluid Dynamics and Laser Conf., Honolulu, HA, June 8 1987.
9. D.A. Kirkpatrick, G Bekefi, A.C. DiRienzo, H.P. Freund and A.K. Ganguly , "A millimeter and submillimeter wavelenght free-electron laser" *American Institue of Phyics Fluids*, B1 (7), July 1989.

THIS PAGE INTENTIONALLY LEFT BLANK

INITIAL DISTRIBUTION LIST

1. Defense Technical Information Center 2
 8725 John J. Kingman Rd., STE 0944
 Ft. Belvoir, VA 22060-6218

2. Dudley Knox Library 2
 Naval Postgraduate School
 441 Dyer Rd.
 Monterey, CA 93943-5101

3. Professor William B. Colson, Code PH/Cw 4
 Naval Postgraduate School
 Monterey, CA 93943-5117

4. Professor Robert L. Armstead, Code PH/Ar 1
 Naval Postgraduate School
 Monterey, CA 93943-5117

5. Lieutenant Daniel S. Massey, USN 2
 17026 Virginia Ave
 Willamsport, MD 21795

6. Dipl.-Phys. Sergiy Khodyachykh 2
 Institut fur Kernphysik
 Scholbgartenstrabe 9
 Darmstadt Germany D-64289